ASTRONOMY IN THE REGION 1-0.1 mm WAVELENGTHS

National Aeronautics and Space Administration

Grant NGR 22-009-526

SEMIANNUAL REPORT

covering the period

January 1, 1971 - September 30, 1971

(including additional three months no-cost extension)

Submitted by : Rainer Weiss

February 7, 1972

Massachusetts Institute of Technology
Research Laboratory of Electronics
Cambridge, Massachusetts 02139

Balloon Measurements of the Far Infrared Background Radiation *

Dirk Muehlner and Rainer Weiss

Department of Physics and the Research Laboratory of Electronics

Massachusetts Institute of Technology, Cambridge, Massachusetts 02139

Measurements in five different passbands in the spectral region below 20 cm^{-1} have been made with a liquid helium cooled radiometer in two flights at approximately 40 km altitude. The equivalent temperatures are $2.7\ ^{+.4}_{-.2}$, $2.8 \pm .2$, $2.8 \pm .2$, ≤ 2.7, ≤ 3.4 °K in passbands of 1 to 5.4, 7.8, 7.9, 11.1, and 18.5 cm^{-1}. The results are consistent with a 2.7°K thermal radiation background. Atmospheric radiation of uncertain magnitude dominates the region above 11 cm^{-1}.

INTRODUCTION

The discovery in 1965 of the isotropic background radiation by Penzias and Wilson[1] and its subsequent interpretation by Dicke et al.[2] as the redshifted remnant of the thermal radiation of a primordial cosmic fireball opened one of the most fascinating areas in observational cosmology.

Gamow[3] in his work in the early 1950's on the origins of the universe had alluded to this radiation but had not stressed the fact that it might be observable. This is probably the reason why his calculations had been forgotten by 1965.

Ground based measurements[4,5] in the region between 0.1-3 cm^{-1} have been consistent with the interpretation that the universe is filled with black body radiation at 2.7°K. Also, extensive measurements[6,7] of the isotropy of the radiation at 0.33 cm^{-1} have lent additional support to the cosmic hypothesis.

Although the existence of an isotropic microwave background radiation is well established, the crucial questions of whether the spectrum is truly thermal and also whether the radiation is indeed isotropic in the region where it has maximum spectral brightness remain unanswered.

The spectral peak of a 2.7°K black body lies at approximately 6 cm^{-1}. This is a miserable region of the electromagnetic spectrum in which to carry out experiments. The technology of far infrared detection is in a primitive state; furthermore, even if this situation is eventually improved, any background measurements in this region are complicated by the inevitable radiation from sources that are at temperatures

considerably higher than 3°K.

Radiation by the earth's atmosphere is sufficiently strong to preclude any direct ground based measurements in the region above 3 cm^{-1}. This leaves the field to balloon, rocket or spacecraft observations, or to indirect techniques such as measurements of the distribution of rotational states of interstellar molecules by absorption spectra of the interstellar medium[8,9].

Since 1967 several groups have carried out direct measurements in this region[10,11,12,13,14] using rocket and balloon borne instruments.

This paper describes a balloon experiment designed to make a direct measurement of the background radiation in the region from 1 to 20 cm^{-1} and presents the results of two balloon flights made on June 5, 1971 and September 29, 1971, from the balloon facility of the National Center for Atmospheric Research (NCAR), Palestine, Texas.

APPARATUS

The design of a balloon borne radiometer to make an absolute measurement of the isotropic background spectrum in the far infrared is constrained in several ways. First, radiation from the optical components of the radiometer should not greatly exceed the incoming radiation. In practice this means that all the optical components must be held at liquid helium temperatures. In fact in this experiment the optics are immersed in liquid helium.

A second constraint is imposed by the poor detectors available for the far infrared region. A detector with an area of about 0.1 cm^2, for example, is typically able to detect a minimum of $\sim 10^{10}$ photons in one second. The optics must therefore have as large a solid angle-area product as is practical; in the apparatus described in this paper it is

approximately 0.3 cm^2 sr.

At the same time the radiometer beam must be narrow enough in angle to permit measurements of atmospheric radiation by zenith angle scanning and also small enough in cross section to enter the liquid helium dewar without being intercepted by surfaces at ambient temperature. The opening in the dewar cannot be made very large without incurring prohibitive losses of liquid helium.

A typical flight may last one half day during which time the instrument must remain immersed in liquid helium. This is ensured by enclosing it in a sealed copper can surrounded by a reservoir of liquid helium which is allowed to evaporate into the atmosphere and thereby provides refrigeration. The liquid helium in the sealed can is used only as a thermal conductor. Because liquid helium shrinks by a remarkable 15% between 4.2°K and 1.5°K, the entrance window to the radiometer can is recessed so that it will always be in contact with the liquid.

Finally, some provision must be made to separate the atmosphere at low altitudes from the liquid helium, since otherwise the radiometer would be covered with air and water frost. This separation is provided by two gas-tight but transparent covers which are removed during the course of the experiment. A schematic drawing of the apparatus is shown in Figure 1.

The principal optical components of the radiometer are the cold window, the interference filters, the Teflon lens, the collimating cone, the beam chopper and the detector. The optical properties of these components are described below.

Collimation of the radiometer beam is accomplished by a cone-lens combination consisting of an aluminum condensing cone with a Teflon lens

mounted at the top. The lens is designed to have its focal point at the vertex of the cone. In the limit of geometric optics[15,16] the cone-lens system is an ideal condenser of radiation; it illuminates the lower opening with radiation from a full 2π solid angle while accepting radiation at the upper opening only from the solid angle allowed by energy conservation. In other words, it is an f/0 condensing system which conserves the solid angle-area product of the beam passing through it. The major constraint on the design of the cone is the size of the detector, which fixes the diameter of the lower opening. The size of the upper cone opening is determined by the best compromise between beam diameter and divergence. The cone used in the experiment has a lower opening of 0.5 cm diameter and an upper opening of 5.5 cm. The beam half angle is about 5° by geometric optics.

A filter disk with six evenly spaced openings is located above the collimating cone. One of the six openings is filled with a transparent Teflon sheet, four openings are occupied by low pass interference filters, and the sixth position is blocked off by a sheet of copper. Any of the six filter positions may be selected by rotating the disk, which is turned by a rotary solenoid operating in the liquid helium. An absorber composed of iron filled epoxy surrounds the radiometer beam in the region of the filter disk and blocks off indirect paths by which scattered radiation might bypass the filters.

Far infrared transmission spectra at 4.2°K of some of the components in the optical train, as well as the spectral response of the detector, are shown in Figure 3. All spectra were measured using a far infrared interferometer.

The transmission spectrum of a sample is found by dividing a spectrum taken with the sample in place by a "background spectrum" taken with the sample removed. The ratio is not affected by the spectral characteristics of the interferometer and detector. The spectral response of the detector is difficult to determine absolutely. We have used several approaches. First, we have compared an InSb detector to a germanium bolometer (Texas Instruments) by using both with the same interferometer. It is generally assumed that the germanium detector has a flat spectral response in the far infrared. The spectral response of InSb determined this way is shown in Figure 3. Second, we measured the reflectivity and transmission of a sample of InSb at 4.2°K. The reflectivity is frequency independent while the transmission increases with frequency. Assuming that the power absorbed is proportional to the signal developed, these measurements give the spectral response of the detector. The results are consistent with the spectrum found by comparing the InSb and germanium detectors. Finally, the black body calibration of the entire instrument, which will be described later, appears to confirm the adopted detector response.

The dominant high frequency roll-off for the instrument is determined by the cold window and the detector response. The cold window is opaque from about 40 cm^{-1} on through the visible region of the spectrum. Spectral resolution is provided by a set of capacitive grid, low pass interference filters similar to those described by Ulrich[17]. A detailed account of the construction of rugged filters of this kind which can be used at low temperatures was given in a previous report[18].

The low frequency cut-off of the instrument is due to the collimating

cone. The cut-off frequency of the cone is too low to be easily measured directly, and so the approach we took was to measure the cut-off characteristics of small scale models of the actual cone. We found as expected that these cones exhibited sharp cut-offs at frequencies inversely proportional to the sizes of the cones. The cut-off of the cone used in the experiment is at $\sim$1 cm^{-1}.

The five spectral responses of the entire instrument are shown in Figure 4. $\overset{(one)}{SR1}$ is composed of the product of the spectral response of the cold window, collimating cone, Plexiglass chopper and detector. SR2 through SR5 are obtained by multiplying $\overset{(one)}{SR1}$ by the appropriate interference filter transmission spectra.

The response curves are normalized at low frequencies. The vertical axis may be calibrated for each spectral response by multiplying by the calibration factor shown in the figure.

Figure 5 shows the same five responses multiplied by the frequency squared, and shows better than Figure 4 how the instrument responds to high temperature thermal source spectra. The "equivalent box bandwidths" listed in both Figures 4 and 5 show the high frequency cut-offs of ideal square box filters which would give the same response to white and ν^2 spectra as the actual responses $\overset{(one)}{SR1}$ - SR5.

The beam profile of the radiometer was measured with the instrument in its flight configuration except that a 0.005-cm thick sheet of polyethylene was substituted for the Mylar membrane and cover. The measurement was carried out by moving a modulated mercury arc source across the radiometer field of view at a distance of $\sim$2-1/2 meters from the cold window. The beam profile of the radiometer measured in this manner for

each spectral response is shown in Figure 6. It is evident that the angular distribution depends on the spectral response; the radiometer beam widens with decreasing cut-off frequency. This appears to be a diffraction phenomenon which most likely occurs in the collimating cone. The polyethylene sheet also causes a systematic broadening of the angular distribution which, unlike the diffraction broadening, increases with increasing frequency. This comes about by multiple reflections of the radiometer beam between the polyethylene sheet and the conical radiation shield at the entrance to the radiometer. Since all the covers are removed during the flight, the angular distributions shown in Figure 6 give upper limits for the weak large angle tails of the actual distributions.

Figure 7, which is derived from the data of Figure 6, shows the response of the radiometer to a ring source of constant linear intensity everywhere at an angle θ to the optic axis, as well as the integral of this quantity from 0 to θ. The limiting value of the integral may be interpreted as the effective solid angle of the radiometer beam in each spectral response; note that the values tabulated for these "effective solid angles" depend on the normalization of the point source response to unity at $\theta=0$, as shown in Figure 6.

Since the radiometer beam does not have a sharp cut-off, it is necessary to shield the radiometer from hot sources at large angles. In particular, the radiometer should not see any reflections of the hot ground and lower atmosphere. Inadequate precautions in this respect may have been the most serious flaws in the 1969 flight of the first apparatus[14]. The main purpose of the inner cone shown in Figure 1 (one) is to ensure that

only the sky will be reflected into the radiometer at large beam angles. It is further necessary to minimize the thermal emission of radiation by the cone itself.

The cone extends from a region at ambient temperature to the top of the sealed can which is at liquid helium temperature. In order to minimize the heat flow into the dewar, the cone is constructed of 0.013-cm stainless steel, a metal of high emissivity. To reduce its emissivity the cone is gold-plated and then coated with a 0.01-cm thick layer of Teflon. This dielectric layer reduces the emissivity at grazing angles, which for bare metal surfaces is dramatically larger than at normal incidence. The calculated emissivity of the cone over the frequency range of the radiometer is less than 0.0025 at all angles.

In order to estimate the cone's contribution to the radiometer signal, it is necessary to know what fraction of the total beam is intercepted by the cone in each spectral response. This was measured by moving a modulated mercury arc source across the radiometer beam at a height level with the top of the cone, but with the cone removed. The results are 0.92%, 2.5%, 2.15%, 3.15%, and 6% for SR1 (one) through SR5. The top of the cone has a diameter of 26 cm.

In order to keep contaminants such as moisture, dust, ballast and

air out of the instrument, it is protected by two sheets of Mylar which cover the opening at the top. The covers are stretched on hoops mounted by spring-loaded hinges and may be flipped out of the way of the radiometer beam by burning through nylon fastening lines. The outer cover is a 0.0025-cm thick sheet of Mylar which makes a gas-tight seal to the outer cone. This cover stops the bulk of the moisture, dust and ballast, and is removed early in the flight. The inner cover, or membrane, is mounted in the same way as the outer cover. It consists of a 0.00025-cm thick sheet of Mylar and forms a gas-tight seal to the top of the inner cone. The membrane serves to keep air out of the instrument both during the ascent and at float. More will be said about it in the description of a flight.

An important requirement for the covers is that they be transparent in the far infrared so that measurements can be made during the ascent, and so that in the event of failure of the cover-release mechanism a flight is not a total loss. In an investigation of cover materials we measured the absorption length in thick sections of Mylar and polyethylene at 300°K in the spectral region characteristic of SR1 (cone). The absorption length in polyethylene was ∿8 cm while for Mylar it was ∿0.3 cm. From these measurements the emissivities of the Mylar cover and membrane are calculated as 8×10^{-3} and 8×10^{-4}. Radiation due to reflection of the dewar and cone by the cover and membrane is negligible compared to emission. In the June flight we used polyethylene covers but we experienced some difficulties described later. In the September flight we used Mylar because of its superior mechanical properties.

The detector used in the experiment is an InSb hot electron bolometer first described by Rollin[19]. Detectors were cut on a string saw from a boule of undoped n-type InSb. The boule had the following specifications at 77°K: carrier concentration, $6 \times 10^{13}/cm^3$; Hall mobility, 5×10^5 cm^2/volt sec; and resistivity, 0.3 ohm cm. After being cut into chips of about 5 X 5 X 1/2 mm, detectors were etched in a standard CP-4 solution. Gold leads were attached to the chips using indium doped with sulfur or tellurium as solder. The assembled detectors were tested for their responsivity and noise characteristics. In the course of these studies, we found some simple criteria for bad detectors. Detectors which displayed asymmetric V versus I curves with current reversal, or had unusually high impedances, generally proved to be noisy. Non-ohmic or otherwise poor contacts are probably responsible for this.

A good detector usually had a dynamic resistance of 100 ohms or less at the optimum operating point, which was usually at bias currents between 0.1 and 0.5 ma and near the knee of the V versus I curve. A good detector shows no increase in noise when the bias current is turned on. The V versus I curves at 4.2°K and 1.8°K for the detector used in the radiometer are shown in Figure 8.

A major problem with InSb detectors, because of their low impedance, is to match them to amplifiers so that the amplifier noise is smaller than the thermal noise generated in the detector. At present the best field effect transistors, such as the 2N 4867A used in the detector preamplifier, typically have a voltage noise of $\sim 5 \times 10^{-9}$ volts/$Hz^{1/2}$

and a current noise of $\sim 5 \times 10^{-15}$ amp/Hz$^{1/2}$ at frequencies above 100 Hz. The thermal noise of a 100Ω InSb detector at 4°K is approximately 2×10^{-10} volts/Hz$^{1/2}$. A liquid helium cooled stepup transformer is a straightforward way to make the impedance transformation. Unfortunately, we found ferromagnetically-coupled transformers and inductors to be microphonic and their windings to have a tendency to break on thermal cycling. We use a series RLC stepup circuit employing a 2.7-henry air core inductor wound with copper wire on two nylon dees. The dees are arranged as sections of a toroid to reduce pickup from external magnetic fields. The coil is enclosed in a superconducting magnetic shield and potted in mineral oil to reduce microphonics. The tuning capacitor is across the FET preamplifier input. The Q and therefore the voltage stepup of the RLC circuit is 50. The overall noise voltage of the system with the chopper turned off is roughly twice the thermal noise of the detector at 4°K.

Figure 8 shows the synchronously detected output signal of the detector when irradiated by a modulated mercury arc as a function of the bias current. The curves at 4.2°K and 1.8°K both show responsivity versus bias current with and without the stepup RLC circuit. They display the increase in detectivity with decreasing temperature as well as the loading of the detector by the RLC circuit.

At 1.5°K the responsivity is ∼200 volts peak to peak per watt incident on the detector. Assuming the detector noise to be twice the 4°K thermal noise, this gives the detector a noise equivalent power of $\sim 2 \times 10^{-12}$ watts/Hz$^{1/2}$.

The final element of the optical train which deserves some comment

is the chopper. The chopper is a 3/4-mm thick Plexiglass disk divided into 22 wedge-shaped sections in which alternate sections are aluminized. The disk, driven by an external synchronous motor, rotates at 30 Hz in a slot cut into the collimating cone 1-1/2 cm above the detector. The chopper exposes the detector alternately to the incoming radiation and the thermal radiation in a closed cavity at the helium bath temperature. A frequency reference signal is derived from the chopper drive shaft near the motor.

In order to overcome the 1/f noise in the preamplifier as well as to allow small electrical components to be used in the stepup and amplifier circuitry, it is desirable to use as high a chopping frequency as possible. However, this aggravates the substantial microphonics problem created by the chopper moving in the liquid helium. The chopper rim speed exceeds the critical velocities in superfluid helium by several orders of magnitude. Even in the normal fluid the chopper creates a flow with a very high Reynolds number, producing turbulence. Since the signals to be measured are of the order of 10^{-9} to 10^{-10} volts, such things as the vibration of leads in the earth's magnetic field and the change in capacitance of coaxial lines due to vibrations generate objectionable noise voltages if they are not controlled. While InSb is both piezoresistive[20] and piezoelectric[21], it seems most likely that the dominant microphonic signals come from the temperature fluctuations which accompany pressure fluctuations in the liquid helium. The detector is mounted in a completely enclosed volume to reduce these fluctuations. We have not been completely successful in eliminating the microphonics problem. The microphonic noise remains the dominant noise in the

experiment, being about 5 to 10 times larger than the thermal noise.

In the construction of the apparatus we have used various commercially available devices and materials which may be useful to others involved in cryogenic technology. Among these were the following:

"Fluorogold" (Fluorocarbon Company, Pinebrook, N.J.), the material used as the cold entrance window of the radiometer, is a glass-filled Teflon which serves both as a low pass filter in the far infrared and as a gasket for vacuum seals at cryogenic temperatures.

Chempro "O" rings (Chemical & Power Products, Inc., Cranford, N.J.), which can best be described as screen door springs enclosed in Teflon tubing, make reliable and thermally recyclable vacuum seals between smooth surfaces.

Cajon (Cajon Company, Solon, Ohio) fittings using replaceable nickel gaskets are useful in making seals that have to be opened or closed while at liquid helium temperatures.

"Bartemp" stainless steel ball bearings (Barden Corporation, Danbury, Conn.) operate well at low temperatures. Lubrication for the bearings is provided by Teflon ball separators impregnated with molybdenum disulfide. We use them to mount the chopper disk and in a gimbaled bearing located near the middle of the chopper shaft to prevent whipping of the shaft.

Ledex rotary solenoids (Ledex, Inc., Dayton, Ohio) operate well in liquid helium without any alterations. In conjunction with Torrington one-way clutches (The Torrington Company, Torrington, Conn.), which have to be degreased before use, the rotary solenoids make simple stepping motors.

The 330 Hz detector signal, after passing through the low noise preamplifier, is amplified further and converted into a DC output voltage in the conventional way by a lock-in amplifier. The noise bandwidth of the amplifier is determined by the output filter which provides a double integration with a time constant of 2 seconds.

An automatic way of accommodating the more than three orders of magnitude signal variations which occur in the flight is provided by a gain switch which selects one of seven discrete gains, covering a total range of a factor of 1000 in steps of $\sqrt{10}$. The switch is controlled by the lock-in amplifier output voltage and changes the gain when the output becomes less than 0.2 V or greater than 0.9 V for several seconds. The system is linear in any gain setting.

The radiometer dewar is attached to the frame of the balloon package (see Figure 11) on two pillow blocks. By means of a gearmotor the zenith angle of the radiometer beam may be varied between $\sim$1° and $\sim$45°. The zenith angle of the radiometer beam is measured by a pair of pendulous accelerometers fixed to the dewar. In this way the angle with respect to true vertical is measured irrespective of the orientation of the rest of the balloon package. The azimuth of the radiometer beam is not controlled; however, it is measured by a pair of Hall probes which sense the components of the earth's magnetic field in two orthogonal directions.

A small black body used to monitor the performance of the radiometer during a flight is located at the top of the dewar assembly. This "inflight calibrator" consists of a conical piece of iron-filled epoxy of the same type used in the laboratory calibrator. Its temperature is not controlled, but is measured by a wide range resistor-thermistor

combination. The black body is suspended by three thin wires at the center of a U-shaped hoop of thin walled stainless steel tubing large enough to clear the radiometer beam. The whole assembly is mounted on a velocity-controlled rotary solenoid which when activated moves the black body into the center of the radiometer beam. The position of the inflight calibrator is read out by a potentiometer mounted with the rotary solenoid.

A motor-driven camera is mounted on a post near the back of the balloon package and overlooks the top of the dewar. The camera is equipped with twelve flashbulbs for illuminating the apparatus during the darkness of a night flight, and can take that many pictures on 35 mm film.

The information gathered throughout the flight is telemetered to the ground as well as recorded on an onboard tape recorder. One multiplexed channel carries the most essential information coming from the instrument, such as the lock-in amplifier output, gain setting, filter position, zenith angle, azimuth, calibrator temperature and position, and various temperatures in the dewar. Another multiplexed channel carries housekeeping information. A multiplex commutation cycle lasts 15 seconds and is divided into 30 sections. The radiometer output is sampled every 1.5 seconds, providing an essentially continuous record.

CALIBRATION

Given the spectral response curves shown in Figure 4, a single measurement of the response of the radiometer in each spectral response, using a known source spectrum, would constitute a complete calibration of the instrument. In other words, this would fix the vertical scale of Figure 4 in volts per unit flux for each spectral response. Our

faith is not that strong, however, and so we calibrated the instrument by exposing it to black body radiation over a wide range of temperatures down to ∿3°K. Figure 9 is a schematic drawing of the black body used for this calibration. The calibrator sits immediately above the cold window through which the radiometer looks out at the world. The part of the calibrator which is actually black is a cylinder of iron-filled epoxy (Eccosorb MF-110, Emerson & Cuming, Inc.) with a conical hole in it. Measurements made on this material at 4.2°K with a far infrared interferometer showed it to have a reflectivity of about 10% between 10 cm^{-1} and 60 cm^{-1}, and also to be a strong absorber in thicknesses characteristic of the piece in the calibrator. The Eccosorb black body is matched to the radiometer by an aluminum cone, which optically magnifies it so that it almost completely covers the radiometer beam. The Eccosorb is mounted in a thick-walled OFHC copper "oven" which is heated by ten resistors symmetrically arranged in holes in the copper, and cooled by the cold helium gas in the dewar. The temperature is measured by a carbon resistor thermometer which was calibrated through a continuous range of temperatures determined by helium vapor pressure below 4.2°K and a commercial germanium resistance thermometer above 4.2°K. Both thermometers were checked at the discrete reference points provided by the boiling points of helium, hydrogen, nitrogen and oxygen. The oven is insulated from the aluminum cone by a Teflon spacer. The temperature of the aluminum matching cone is never greater than that of the oven, and since the aluminum is a good reflector it has a negligible effect on the radiation seen by the radiometer.

Figure 10 shows the reduced calibration data, in the form of detector voltage versus calibrator temperature. The solid curves in the figure are computer calculations based on the spectral responses of Figure 4. These curves are the frequency integrals of the spectral responses times the Planck black body spectrum at each temperature. The fit between the measured calibration points and the calculated curves has only one free parameter, the overall system gain, which is a common factor for all spectral responses.

The bulk of the calibrations were performed in a large environmental chamber at the Avco Corporation facility in Wilmington, Massachusetts, in which the apparatus could be pumped down to a pressure of 2.5 mm Hg. At this pressure, which is equal to the pressure at flight altitude, liquid helium is at 1.5°K. For several reasons it is important to know how the response of the radiometer changes with helium bath temperature. For example, the preflight calibrations are performed at 4.2°K. Also, during the ascent the liquid helium temperature changes continuously from 4.2°K to 1.5°K and finally, at the end of the flight, useful data can be obtained even though the apparatus may no longer be at 1.5°K. There are two ways in which the bath temperature affects the calibration. First, the responsivity of the detector increases with decreasing temperature. However, the detector resistance increases as well, so that the net effect when the loading of the RLC circuit is included is not large. The system gain increases by a factor of 1.4 between 4.2°K and 1.5°K. It is important to note that the measured spectral response of the InSb remains unchanged between these temperatures.

The second effect is more subtle. The AC detector signal is

proportional to the difference between the power absorbed by the detector when the chopper is open and when it is closed. When the chopper is closed the detector is bathed in radiation at the temperature of the radiometer as determined by the liquid helium bath. The observed signal due to an outside radiation source is therefore smaller than it would be for a radiometer at zero temperature. Indeed, if the temperature of the outside source were equal to that of the radiometer, no signal would be developed, and for an even colder source the signal would reverse phase. The dependence of the detector signal on the radiometer temperature is given by

$$V_{det.} \propto \int R(\nu)[B_{out}(\nu) - B_{rad.}(\nu,T)]d\nu.$$

$B_{rad.}$ is the spectral brightness of a black body at the radiometer temperature T, B_{out} is the spectral brightness of the exterior source, and $R(\nu)$ is the spectral response function of the radiometer.

The most useful way to correct measured data for different radiometer temperatures is first to reduce the calibration data to an idealized radiometer temperature of 0°K, which has been done in Figure 10. This procedure requires some trust in the measured spectral responses. The correction that should be added to the signal due to an outside source with the radiometer at a temperature T can now be read off of the calibration curve for each spectral response directly.

A final problem in interpreting the calibration data is that the Eccosorb as reflected in the calibrator cone did not quite fill the whole radiometer beam. The effect of this is that when an actual measurement of radiation from the sky or from the room is compared to the

calibration data, it must first be multiplied by a factor equal to the ratio of the solid angle of the whole beam to that covered by the calibrator. These factors are determined by comparing the signals in the different spectral responses due to the black body calibrator at 80°K with those due to the room, an excellent black body at ~300°K. Both temperatures are in the Rayleigh-Jeans range for all spectral responses. The factors are 0.81, 0.73, 0.68, 0.65, and 0.59, for SR1 through SR5.

FLIGHT TRAIN AND DESCRIPTION OF A FLIGHT

The flight train had the following components in both the June and September flights. At the top is a Raven Industries 11.7 million cubic foot balloon of 0.0007-inch polyethylene, which by itself weighs 1360 pounds. Suspended below the balloon by its own parachute is a reel which carries 2000 feet of 3/8-inch nylon line and lowers the scientific payload away from the balloon in flight. A telemetry package including a radiosonde and tracking beacon as well as the command system for the letdown reel is mounted on the reel framework. The scientific package hangs by its parachute at the bottom of the 2000-foot nylon line from which it is cut loose, when the flight is terminated, by a squib. The scientific telemetry is in a separate box which rides on top of the instrument package. Below the package is a crush pad of corrugated cardboard.

The reel increases the probability of failure of the balloon flight and complicates the flight as well. The reel has been tested for payloads of approximately 500 pounds. The scientific package and its

telemetry, parachute and rigging in our flights weigh ~500 pounds and therefore leave no margin. The present state of the ballooning art, however, requires that it be possible to decrease the weight of the flight train as the balloon traverses the troposphere where the atmospheric temperature is at a minimum. In this region there is a tendency for balloons to reduce their ascent rate and, in effect, get stuck. One might think that by increasing the free lift on the ground, this could be avoided. However, there is a constraint on fast ascent rates imposed by the thermal shock on the balloon as it enters the troposphere.

The solution used at present is to carry some disposable ballast, typically 10% of the total flight train weight (200 pounds in our case), that is released while the balloon is in the troposphere and the lower stratosphere. In both flights, the ballast was carried in ten bags mounted on a beam placed just above the reel. These bags are ruptured on command, releasing the ballast which is a steel powder of approximately Gaussian distribution with a 0.013-inch diameter mean and 0.004-inch variance. By the time the ballast reaches the payload it is dispersed over a large area; nevertheless, several particles strike each square centimeter of the payload. The outer cover on the radiometer protects the instrument against this shower. In the June flight, however, at least one of the larger ballast particles did manage to pierce the outer cover and, by a sequence of events to be described later, shattered the membrane. For the September flight we sieved the ballast to exclude particles with diameters larger than 0.015 inch.

Once ready for flight--batteries charged, telemetry and payload checked out--the apparatus is stored warm and we wait for good weather. We require a prediction at 11 a.m. or earlier on the day we fly of a reasonable chance of surface and low level (~500 feet) winds less than 12 knots, less than 10% cirrus cloud cover, no cumulus clouds, and little chance of afternoon thunderstorms. If these conditions are "promised" we pump out the sealed copper can and fill it with helium gas that has been passed through a liquid nitrogen trap to remove water and oil. Next we begin the struggle against frost formation. During the nitrogen and helium transfer the storage dewar is clothed in two nested polyethylene bags that isolate the apparatus from the room atmosphere. These bags are in addition to those shown in the schematic of the apparatus (Figure 1). Dry nitrogen, the efflux from liquid nitrogen, is circulated through the storage dewar for approximately 1/2 hour. Then liquid nitrogen is transferred into the storage dewar until approximately 3 to 4 liters have accumulated. The transfer is stopped and a heater located at the bottom of the storage dewar is turned on to maintain a positive pressure of dry nitrogen in the bags as well as to produce a cold gas flow past the copper can and cones. At this point, a second weather briefing is given to reassess the possibilities for a flight before we transfer the liquid helium. If the weather still looks favorable, the liquid nitrogen is removed by boiling it out with increased power in the heater. After the nitrogen is exhausted the storage dewar is flushed with clean helium gas and the liquid helium transfer begins through the two polyethylene bags. At this point the membrane which makes a gas seal to the inner cone is tightened down. As soon as a liquid helium level has been established,

the seal in the copper can is opened and the liquid helium transfer tube is inserted into the copper can. The remainder of the filling operation is performed in this configuration until both the copper can and the storage dewar are filled to capacity (approximately 55 liters). The entire transfer requires about 85 liters of liquid helium. The transfer tube is removed, the copper can is sealed once again, and the holes for the transfer tube in the two polyethylene bags are sealed. After the outer parts of the apparatus have come back to room temperature, the bags are removed and the outer cover is installed. A flow of clean helium gas is maintained in the region between the outer cover and the membrane. Next the inflight calibrator is installed. A preflight calibration in all filter positions is performed, using the 300°K room radiation. The package is now turned over to the NCAR crew for final rigging on the launch vehicle.

A final checkout is performed in the field; if this is successful and if the weather is still satisfactory, the balloon is inflated.

At launch the dewar is tipped so that the optic axis of the radiometer is 20° from the zenith. The flight train begins to ascend at a rate of about 900 feet/min., a rate which is maintained during most of the ascent. At an altitude of 5000 feet the deployment of the 2000-foot line begins. The entire deployment takes approximately 20 minutes. After deployment of the line, the telemetry transmitter for the reel is turned off and a study of the RF interference from the remaining sources begins.

Although the RF immunity studies can begin on the ground, the actual flight configuration of the antennas of course cannot be duplicated. RF

interference due to the 1.7-mHz beacon is easy to determine since we can turn it off at will and note if there is an effect on the radiometer output. Determining the RF interference from the 235-mHz payload telemetry is more difficult, since the telemetry is our only link to the experiment during the flight. One scheme we employ is to send a command that attenuates the transmitted power by one-half and look for a change in the radiometer output. This is done throughout the flight but especially at float altitude when the radiometer signals are small. This procedure is used for diagnostic purposes only. Throughout the flight we have periods when we turn the telemetry off entirely and rely on the onboard tape recorder so that in case there is RF interference we have some data that are RF-free.

Although we had considerable difficulty with RF interference in the flight made in September 1969, there was no problem in either of the 1971 flights.

Some of the measures we took to avoid RF interference are listed below.

All leads that communicate between the inside of the electronics compartment and the outside world pass through π section RF filters. The electronics compartment itself has finger stock gaskets on the doors. The leads in the signal circuitry run in double-shielded coaxial cables. Finally, the telemetry antenna hangs below the package by a 30-foot cable. The antenna is a 1/2 wave dipole with a ground plane oriented so that the apparatus is in the antenna's cone of silence.

The various temperatures of the inner cone are monitored continuously during the ascent, since an abrupt drop in temperature would

indicate that the membrane had ruptured. This might occur shortly after a command to release ballast is given, as happened in the June flight.

During the ascent and throughout the flight, photographs of the top of the dewar are taken by the onboard camera; some of these are shown in Figure 12. These pictures show such things as the positions of the cover and membrane, the frost accumulation and the operation of the inflight calibrator.

As soon as all the ballast has been released, we remove the outer cover. This is verified in flight by a signal from a microswitch actuated by the cover frame and also by a change in the radiometer output voltage. In the September flight the reduction in radiometer signal when the cover was removed was 1.09×10^{-7} r.m.s. detector volts in SR1. This value is within a factor of two of that calculated using the measured absorption coefficients of Mylar and the ambient temperature.

At float altitude we begin a program of zenith scanning which is carried out in two ways. One way is to hold the zenith angle fixed and go through the entire filter sequence quickly, calibrating once in each filter position. The other way is to hold the filter fixed and continuously vary the zenith angle from 1° out to 45° and back again, calibrating at 22° in the return scan. Both of these procedures continue throughout the eight hours that the instrument is at float altitude.

In the September flight the membrane was removed 3-1/2 hours before termination of the flight. This is done in order to determine the radiative contribution by the membrane and also to carry out the experiment without any radiative source directly in the beam.

We had always considered the removal of the membrane, even at flight altitudes, a risky affair. There are still several mm of Hg of air at flight altitude, and it seems reasonable that it would not take long before the cold regions of the instrument would become covered with air snow. The snow most likely would scatter the incoming radiation, affecting high frequency radiation more than the low. We find, however, that nothing happens to the radiometer signals, including the amplitude of the inflight calibration signals, until the liquid helium in the storage dewar has been exhausted. After this, a slowly increasing attenuation which is frequency-dependent does set in.

We inadvertently gained some experience with this phenomenon in the June flight, in which the membrane was opened for the bulk of the flight. In that flight, when the instrument was almost at float altitude, a large ballast particle pierced the outer cover and then shattered a thin polyethylene membrane which at the time was at a temperature of 120°K. The chain of events that followed is amusing but only in retrospect. The draft of cold helium gas released by the broken membrane cooled the outer cover enough to shrink it out of its frame. When the command was given to release the cover, the frame moved but the cover remained virtually in place. Eventually, the inflight calibrator pushed the cover aside and finally the command to release the membrane cleared the entire area at the top of the storage dewar.

The most likely reason why little snow collects in the instrument while there is still helium in the storage dewar is that the helium efflux gas forms a jet in the inner cone when the membrane has been removed. Some independent evidence for this comes from the fact that the inflight

calibrator cools down when it is brought into the field of view after the membrane has been removed. In the September flight the signals contributed by the Mylar membrane were 1.45×10^{-8} and $(3 \pm 1) \times 10^{-9}$ r.m.s. volts at the detector for SR1 and SR2. These are about twice the predicted values.

Both before and after the membrane is removed we attempt to get an estimate of the radiative contributions of the inner cone by changing its temperature. This is accomplished by increasing the flow of helium efflux gas past the cone by turning on a heater in the liquid helium. The temperature of the cone is measured at four locations along its length. If there is a change in radiometer signal which correlates with these temperatures, one can estimate the emissivity of the cone knowing the fraction of the beam that the cone intercepts.

DATA AND INTERPRETATION

This section deals with the data from the September flight and its interpretation. Figure 13 shows a plot of the inflight calibration signals for all spectral responses as a function of time during the flight. The calibrations were performed at many different zenith angles. The data in the figure have been normalized to a calibrator temperature of 100°K; the actual calibrator temperatures range between 250°K and 100°K. The data reveal a 10% change of overall system gain from the beginning to the end of the flight. The points on the right in the figure are the calculated calibration signals at a calibrator temperature of 100°K. These calculations are based on the measured response of the radiometer

to a Rayleigh-Jeans source and the fraction of the radiometer beam covered by the calibrator in each spectral response. The calibrator covers 1.47, 1.18, 0.96, 0.93, 0.81 X 10^{-2} of the total beam in SR1 through SR5.

Figure 14 shows the zenith angle dependence of the signals in the various spectral responses after the membrane had been removed. The data presented are averages for 2 zenith scan sequences and 9 rapid filter sequences at fixed zenith angles. Three corrections have been applied to the original data. First, the offset measured in the blocked position of the filter disk is subtracted from each point. In the rapid filter sequences, the offset measured in the sequence is subtracted from the other points in that sequence. In the scan sequence, the offset scan measured in the blocked position is subtracted from all other scans in the sequence. The offset fluctuates throughout the flight; it is typically a few nanovolts referred to the detector. Second, the averaged signals have been multiplied by the ratio of the solid angle subtended by the primary laboratory calibrator to the solid angle subtended by the entire radiometer beam in each spectral response. Finally, the signals have been adjusted to a radiometer temperature of 0°K. The last two corrections facilitate the comparison of the unknown signals with the calibrations.

The zenith scanning data for SR1 and SR2 show two significant features. The increase in signal at small zenith angles is due to the reflection of radiation from the earth and the lower atmosphere by the 0.0018-cm thick polyethylene balloon. Emission of radiation by the balloon is small in comparison. The balloon subtends 6° at the radiometer. When near the

center of the radiometer's field of view it contributes a signal of 160, 17, 5.5, and 5.2 nanovolts in SR1, SR2, SR3 and SR4. The balloon contribution is calculable at all angles but becomes negligible relative to the observed signals for zenith angles greater than 20°.

The second feature in the zenith scanning data of SR1 and SR2 is the slow increase in signal with angle for large zenith angles. We attribute this to the atmosphere; it is a larger effect in SR1, which includes more atmospheric emission lines, than in SR2. The signal to noise ratio in SR3, SR4, and SR5 is not good enough to determine a zenith angle dependence.

Unfortunately, the actual atmospheric contribution to the total radiometer signal is not determined uniquely by the variation of the signal with zenith angle. A detailed model for the atmospheric radiation is required. The only model independent calculation that can be made directly from the data is an estimate for the lower limit of the atmospheric contribution.

If the temperature and composition of the atmosphere are only a function of altitude, $\sec\theta$ gives the strongest possible dependence of the atmospheric radiation on zenith angle. The limiting case of $\sec\theta$ occurs when the radiation sources are at low enough altitudes so that the curvature of the atmosphere can be neglected, and if in addition the atmospheric emission lines are unsaturated. This means that the spectral brightness at the emission line center is much less than the spectral brightness of a black body at the temperature of the atmosphere. For other cases the atmospheric radiation varies more slowly with zenith angle. For saturated lines the total power radiated depends on the line

shape. The total radiation from saturated but narrow pressure-broadened lines with a Lorentzian shape varies as the square root of the number of molecules along the observation path. This corresponds to a $\sec^{1/2}\theta$ zenith angle dependence. Radiation by saturated Doppler-broadened lines would vary still more slowly with zenith angle.

The total voltage across the detector as a function of angle is given by

$$V_T(\theta) = V_{iso} + V_{atm}(0)f(\theta).$$

V_T is the total signal voltage at any zenith angle, V_{iso} is the voltage due to the isotropic component, $V_{atm}(0)$ is the atmospheric contribution at the zenith, and $f(\theta)$ is the atmospheric zenith angle dependence. If we fit the scanning data to the limiting case for which $f(\theta)$ is $\sec\theta$, V_{iso} and V_{atm} are 2.8 ± 0.6 and 9 ± 0.6 nanovolts in SR1, and 0.25 ± 0.7 and 1.5 ± 0.7 nanovolts in SR2. The data cannot be fitted with $\sec^{1/2}\theta$ for the atmospheric dependence in either SR1 or SR2 because this would make the atmospheric contribution to the signal larger than the total measured signal.

The known atmospheric constituents which have emission lines in the region between 1 cm^{-1} and 30 cm^{-1} are O_3, H_2O, O_2, N_2O, CO and OH. Of these ozone, water and oxygen make the largest contributions to the atmospheric radiation at flight altitude.

Figure 15 shows the integrated spectral brightness calculated for each atmospheric constituent at an altitude of 38.5 km, where the atmospheric pressure is 2.5 mm Hg. The assumptions made for each constituent

are discussed below. Appendix 1 describes the theory of the atmospheric calculations.

The ozone lines result from transitions between rotational levels of this asymmetric rotor. The frequencies and strengths of these lines have been tabulated by Gora[22] and by Clough[23]. The lines are weak but numerous; they almost form a continuum. The estimated radiation is based on an average atmospheric temperature of 250°K and the ozone concentrations given in the U. S. Standard Atmosphere Supplements[24]. The assumed column density of ozone is 3×10^{17} molecules/cm^2. There is, however, a substantial uncertainty in this number[25]. The ozone lines are unsaturated.

Radiation by water is also due to transitions between rotational levels. Water is an asymmetric rotor with a complex spectrum. The water line frequencies, strengths and widths have been tabulated by Benedict and Kaplan[26]. The column density of water is uncertain. Over the years, measurements of the mixing ratio of water to air in the stratosphere have varied[27] over a factor of 100. Recent measurements by Murcray et al.[28] give mixing ratios at 30 km between 2 and 3×10^{-6} gm/gm. Gay[29] has measured mixing ratios of the order of 4×10^{-7} gm/gm. We have assumed a column density for water of 3×10^{17} molecules/cm^2, which corresponds to a mixing ratio of 2.5×10^{-6} gm/gm. The strong water lines are fully saturated.

The radiation by oxygen molecules can be calculated with some confidence since the density as a function of altitude is known. The oxygen radiation lines in the far infrared region come from two different transition mechanisms in the molecule. At low frequencies there is a cluster of lines near 2 cm^{-1} and a single line at 4 cm^{-1}. These lines

come from magnetic dipole transitions between states within one rotational level but with different relative orientations of the rotational and electronic spin angular momentum. They have been tabulated by Meeks and Lilley[30]. There is also a set of lines above 12 cm^{-1} which are due to magnetic dipole transitions between different rotational states of the molecule. The rotational spectrum has been tabulated by Gebbie, Burroughs and Bird[31]. The column density of oxygen is 1.4×10^{22} molecules/cm^2. The lines are not completely saturated.

Radiation by N_2O and CO is due to the simple rotational spectrum of a linear molecule in the ground vibrational state. The emission lines and strengths are calculated by standard methods using the molecular constants given in the literature[32]. The column densities are not well known. Seeley and Houghton[33] have established an upper limit of 10^{-7} gm/gm for the mixing ratio of both species above an altitude of 10 km. It is believed that these molecules are generated at the surface of the earth, so that their mixing ratios are unlikely to increase with altitude. Assuming a constant mixing ratio at all altitudes above 10 km sets an upper limit for the column density above 39 km. The resulting column density is 10^{16} molecules/cm^2 for both N_2O and CO.

The estimated OH concentration in the atmosphere, given by Barrett[34] and Leovy[35], is of the order of 10^{12} molecules/cm^2. The radiation that falls into our region arises from λ doubling transitions in rotation states with N=4 or larger. The line intensities are almost independent of frequency and a calculation using the estimated concentration gives the miniscule brightness of $\sim 5 \times 10^{-20}$ watts/cm^2-sr for any line in

our region.

Table I gives the calculated estimates of the atmospheric contributions in each of the spectral responses at an atmospheric pressure of 2.5 mm Hg. The first column lists the assumed conditions. The last row shows the signal one would expect from a 2.7°K black body in each spectral response.

In principle, if ozone and water are the major contributors of atmospheric radiation, it is possible to couple the calculations of the lines in each spectral response with the scanning data. Assuming the ozone radiation to vary with zenith angle as $\sec\theta$, and the water radiation as $\sec^{1/2}\theta$, this would determine separately the column densities of the two constituents, which are the most uncertain quantities. With this information the actual atmospheric contributions to the observed signals, rather than just lower limits, could be established. Unfortunately, the signal to noise ratio in SR2 is not good enough to accomplish this. For a future flight we will make filters for the region between 12 and 20 cm^{-1} which are better suited for these atmospheric measurements.

A further piece of evidence that the atmosphere makes a substantial contribution to the signal at float altitude in SR1 is provided by the variation in signal with altitude in the September flight. During the ascent, the optic axis of the instrument was maintained at 20° to the zenith. The outer cover was removed at a pressure of 4.7 mm Hg. After the removal of the cover the balloon continued to rise until it reached an atmospheric pressure of 2.2 mm Hg, where it remained for a brief period before settling at a pressure of $\sim$2.5 mm Hg.

The radiometer signal followed these variations in altitude. Figure 16 shows the pressure at the instrument as a function of time, and Figure 17 shows the variation in radiometer signal for SR1 during the ascent. The data in this figure have been corrected for changes in detector responsivity with liquid helium temperature. The measured radiative contributions of the outer cover and membrane have been subtracted.

The data clearly show that the atmosphere still makes a contribution to the total signal at 2.5 mm Hg, since the curve of signal versus pressure did not flatten out as the instrument approached flight altitude. Figure 17 shows calculated values of ozone, water and oxygen radiation in SR1 as a function of pressure. The ozone calculation assumes the distribution of ozone given by the U. S. Standard Atmosphere Supplements[24] and as has been mentioned previously this distribution has large fluctuations about the average values given in this reference. Since the ozone lines are unsaturated, the ozone radiation varies directly as the column density above the apparatus. As can be seen from the figure, the signal versus pressure curve could be fitted nicely by just twice as much ozone as has been assumed for this calculation.

Water has been plotted on the basis of a constant mixing ratio of 2×10^{-6} gm/gm and complete saturation of the lines. The oxygen lines are fully saturated for pressures greater than $\sim$3 mm Hg. At pressures smaller than this the lines come out of saturation and the slope of oxygen radiation versus pressure doubles.

In conclusion, although no precise estimates of the atmospheric

radiation can be made from these data, they indicate that the atmosphere is still very influential at 2.5 mm Hg and furthermore that ozone is probably the dominant radiator in the region between 4 and 20 cm^{-1} for altitudes between 20 and 40 km.

At pressures greater than 80 mm Hg or altitudes less than 15 km, the region from the troposphere down to the ground, the radiation is dominated by water with large fluctuations in concentration.

The results of the June flight are given in Table II. Due to the difficulties with the cover and the membrane, the useful data in this flight were obtained in the hour which remained between the time the command to remove the membrane was given and the flight termination. We did not scan to large zenith angles during this time. The data obtained earlier in the flight suffered uncertain effects due to pieces of the membrane and part of the cover which remained in the field of view of the radiometer. For these reasons, the atmospheric contribution was not measured in the flight. The atmospheric corrections given in Table II are the calculated estimates given in Table I. The corrections for the cone are calculated using the measured cone temperatures, the fraction of the beam intercepted by the cone and the calculated emissivity. An important result of the June flight is that the data do not show the large spectral brightness between 10 and 12 cm^{-1} which we had seen in our 1969 flight[14]. The spectral responses SR2, SR3 and SR4 were specifically designed to give spectral resolution around this region.

The results of the September 1971 flight are given in Table III. The atmospheric contributions for SR1 (one) and SR2 are the measured lower limits assuming a $\sec\theta$ dependence for the atmospheric radiation. The atmospheric contributions for SR3, SR4 and SR5 are the calculated

estimates given in Table I. The cone contribution is calculated as for the June flight.

Figure 18 summarizes all known measurements of the background radiation in the far infrared. Direct balloon and rocket observations as well as the indirect measurements based on absorption spectra of interstellar molecules are included.

The center panel shows the results obtained from optical absorption spectra of interstellar gas clouds including CN, CH, and CH^+ by Bortolot, Shulman and Thaddeus[9]. From the distribution of rotation states in these molecules they establish the point at 3.8 cm^{-1} and upper limits at 7.6, 18, and 28 cm^{-1}. Hegyi, Traub and Carleson[36] have seen the R(2) line of CN; they quote a temperature of between 3.6°K and 2.0°K at 7.6 cm^{-1}.

Flux measurements made by broadband radiometers cannot be represented in diagrams such as Figure 18 unambiguously, since they give weighted frequency integrals of the spectral brightness. For the rocket measurements of Shivanandan, Houck and Harwit[10], and Pipher, Houck, Jones and Harwit[12], the spectral brightness shown is found by dividing the total quoted flux by the quoted bandwidth. The results of our balloon experiments and the rocket measurement of Blair et al.[13] are presented using the following procedure. First, we establish for each spectral response an equivalent square box response, in the manner described earlier in this paper. Next, we assume that the signal observed in a spectral response is entirely due to radiation at frequencies within the equivalent box response. In this way a certain amount of

flux is assigned to each spectral region between cut-off frequencies of the idealized responses. This difference between the fluxes is plotted as uniformly distributed in that region. The difference between SR3 and SR4 in the 1971 flights is not shown in the figure. The vertical dimensions of the boxes shown represent the uncertainties due to noise in the observed signals; there is no good way of representing the uncertainty in the entire procedure. The method gives the best results for a smooth source spectrum; a 2.7°K black body spectrum, for example, looks quite reasonable when transformed in this manner.

The upper panel of Figure 18 shows the results of the rocket measurements of Shivanandan, Houck and Harwit and Pipher, Houck, Jones and Harwit, and also those of our first balloon flight in September 1969. For the balloon flight we plot both the total spectral brightness and corrected values based on estimates of the effects of the atmosphere and "hot" parts of the instrument near the radiometer beam.

The middle panel shows both the total and the corrected values of the spectral density in the June 1971 balloon flight. The corrections are based on calculations of the atmospheric radiation.

Finally, the lowest panel displays the results of the September flight. Both the total spectral brightness as well as the upper limits for the isotropic background are plotted. These upper limits are based on the minimum values for the atmospheric contribution as determined from the zenith scanning data.

Figure 19 shows the region of the sky which was observed in the September flight, using equatorial coordinates. The zenith during the time the balloon was at float altitude is indicated, as well as the

region of the sky which was within 45° of the zenith during this period. Much of this area was swept through by the radiometer beam as it scanned through zenith angle and azimuth. The azimuth scanning resulted from torsional oscillation of varying amplitude performed by the instrument package at the end of the 2000-foot line which connected it to the balloon. The average heading about which the package oscillated changed slowly throughout the flight. This equilibrium position of the package was probably fixed by a local wind at the package. The balloon and package both traveled through the atmosphere at the velocity of the wind at the balloon altitude. At the package, 2000 feet below the balloon, the wind velocity may have been different by as much as 10 m/sec, so that the package found itself in a substantial local wind. It is worth noting that such a wind would have carried away local "air pollution" generated by the package.

We cannot set good limits on the isotropy of that part of the signal which can be attributed to background radiation. The signal in SR1 was isotropic to 20% or better; that in SR2 to 40%. For the other spectral responses we can say only that there was no evident dependence of the signal on the part of the sky being observed.

CONCLUSIONS AND DISCUSSION

The uncorrected radiometer signal sets upper limits on the background radiation flux. The flux in SR3, SR4 and SR5 is close to that expected from a 2.7°K black body while in SR1 and SR2 the flux is larger. The uncorrected flux in SR1 is smaller than but comparable to that measured in a similar bandwidth in the rocket experiment of

Pipher, Jones, Houck, and Harwit[12]. The uncorrected flux in SR2 and SR3 indicates, as Blair et al.[13] have also discovered, that there does not appear to be a strong "line" between 10 and 12 cm^{-1} as the results of our first balloon flight in 1969 had implied.

We believe that a substantial part of the flux observed in SR1 and SR2 is due to the atmosphere and cannot rule out the possibility that all of the flux above ~ 10 cm^{-1} is of atmospheric origin. This conclusion is based on the following points. 1) The calculated atmospheric radiation is of the same order of magnitude as the observed flux; we cannot however make a precise calculation of the atmospheric contribution since the column densities of ozone and water are uncertain. 2) The steep slope of the signal vs. pressure curve at flight altitude also suggests a large atmospheric contribution; however this observation cannot be made quantitative without detailed knowledge of the distribution of the atmospheric constituents. 3) The increase in signal with increasing zenith angle yields a model independent estimate of the minimum atmospheric contribution. We have used this estimate to correct the raw flux in SR1 and SR2.

If our interpretation of the excess flux is correct, the measured background spectrum is consistent with a 2.7°K thermal distribution. Our corrected minimum background flux for SR1 of $\leq 2.3 \times 10^{-10}$ W/cm^2 sr is in substantial disagreement with the minimum flux of $1.3 \times 10^{-9} W/cm^2$ sr quoted by PHJH. We have found no explanation for this discrepancy as yet. Harwit [37] has suggested that the increase in signal with zenith angle in our experiment may be due to "earthshine", radiation from the earth and lower atmosphere, which is scattered into the radiometer. This seems

unlikely to us but we cannot rule it out entirely since we have not been able to measure the radiometer beam profile at very large angles.

In a future flight we will make measurements with increased spectral resolution in the region between 12 to 20 cm^{-1}, with particular emphasis on filters that can separate the ozone and water contributions. We also plan to place another baffle around the radiometer dewar to test the earthshine hypothesis.

ACKNOWLEDGMENTS

We are indebted to Richard Benford for his technical assistance in all phases of the experiment. We are thankful for the support offered and interest shown in this experiment by Professor A. G. Hill and Professor B. F. Burke. We are particularly grateful for the Joint Services support of the Research Laboratory of Electronics at M.I.T. as well as for substantial contributions made by the OSSA of NASA, and the Astronomy Branch of the National Science Foundation.

Dr. Nancy Boggess of the OSSA of NASA has been extremely helpful in our effort to carry out this experiment.

The NCAR staff in Palestine is a joy to work with and the success of these experiments is a tribute to their skill.

Table I. Calculated values of the atmospheric contributions in the 5 spectral responses at 39 km altitude. The voltages are given in nanovolts r.m.s. at the detector.

Constituent	Column Density	SR1	SR2	SR3	SR4	SR5
O_3	3×10^{17}	4	0.36	0.034	0.02	0.0015
H_2O	3×10^{17}	2.8	0.11	0.002	0.002	——
O_2	1.4×10^{22}	0.97	0.12	0.06	0.06	0.06
N_2O	10^{16}	Less than 1% of TOTAL ATMOSPHERE				
CO	10^{16}	Less than 1% of TOTAL ATMOSPHERE				
TOTAL ATMOSPHERE		7.8	0.6	0.1	0.08	0.06
2.7°K BLACK BODY		1.3	1.0	0.7	0.7	0.4

Table II. Results of the flight of June 5, 1971.

	SR1	SR2	SR3	SR4	SR5
Total signal at $\theta_z = 25°$ (nV)	15.4 ± 1	$1.5^{+.5}_{-.2}$	$0.6 \pm .3$	$0.7 \pm .3$	$0.35 \pm .2$
Equivalent black body temp. (°K)	$5.6 \pm .1$	$3.05^{+.25}_{-.15}$	$2.6 \pm .4$	$2.7 \pm .4$	$2.5^{+.5}_{-.7}$
Minimum total flux (10^{-10} W $cm^{-2}sr^{-1}$)	$10.3 \pm .7$	$1.05^{+.4}_{-.2}$	$0.43 \pm .2$	$0.55 \pm .3$	$0.3 \pm .2$
Calculated atmospheric correction (nV)	7.8	0.6	0.1	0.08	0.06
Calculated cone correction (nV)	0.2	0.08	0.025	0.03	0.02
Background signal[a] (nV)	7.4 ± 1	$0.8^{+.5}_{-.2}$	$0.5 \pm .3$	$0.6 \pm .3$	$0.3 \pm .2$
Equivalent black body temp. (°K)	$4.3^{+.2}_{-.2}$	$2.6^{+.3}_{-.2}$	$2.5^{+.3}_{-.4}$	$2.6 \pm .4$	$2.5^{+.4}_{-.7}$
Minimum corrected flux (10^{-10} W $cm^{-2}sr^{-1}$)	$4.9 \pm .7$	$0.56^{+.4}_{-.2}$	$0.36 \pm .2$	$0.49 \pm .3$	$0.25 \pm .2$
Normalized box spectral response bandwidth (cm^{-1})	1-18.5	1-11.1	1-7.9	1-7.8	1-5.4

[a]Errors do not include uncertainty in calculated corrections.

Table III. Results of the flight of September 29, 1971.

	SR1	SR2	SR3	SR4	SR5
Total signal at $\theta_z = 25°$ (nV)	12.4 ±.2	1.7 ±.15	.89 ±.15	.85 ±.15	.47 ±.17
Equivalent black body temp. (°K)	5.2 ±.15	3.2 ±.1	2.9 ±.2	2.9 ±.2	2.8 ±.5
Minimum total flux (10^{-10} W $cm^{-2}sr^{-1}$)	8.2 ±.14	1.2 ±.1	.65 ±.15	.68 ±.15	.39 ±.17
Atmospheric correction at $\theta_z = 25°$ assuming secθ dependence (nV)	≥ 9	≥0.9	—	—	—
Calculated atmospheric correction (nV)	—	—	0.1	0.08	0.06
Calculated cone correction (nV)	0.2	0.08	0.025	0.03	0.02
Background signal[a] (nV)	≤3.2 ±.2	≤.72±.15	.77 ±.15	.74 ±.15	.39 ±.17
Equivalent black body temp. (°K)	≤3.4	≤2.7	2.8 ±.2	2.8 ±.2	$2.7^{+.4}_{-.6}$
Minimum corrected flux (10^{-10} W $cm^{-2}sr^{-1}$)	≤2.3	≤0.62	0.56±.15	0.60±.15	0.33 ±.17
Normalized box spectral response bandwidth (cm^{-1})	1-18.5	1-11.1	1-7.9	1-7.8	1-5.4

[a]Errors do not include uncertainty in calculated corrections.

APPENDIX 1

The line strength is given by

$$S = \frac{8\pi^3\nu}{3hc}\left(\frac{N_i}{g_i} - \frac{N_j}{g_j}\right)\left|\mu_{ij}\right|^2,$$

where ν is the frequency, h Planck's constant, c the velocity of light, N_i the number of molecules/cm^2 in the upper state, and g_i the multiplicity. N_j and g_j are for the lower state. μ_{ij} is the matrix element coupling the two states. S in is units of sec^{-1}. If kT is large compared to $h\nu$ the population difference in the two states is approximated by

$$\frac{N_i}{g_i} - \frac{N_j}{g_j} = \frac{h\nu}{kT} Nf,$$

where f is the partition sum fraction in the upper state. If the energy levels involved are rotational states of molecules with $hB/kT \ll 1$, where B is the rotation constant, the partition sum fraction is given by

$$f \approx (2J+1)\frac{hB}{kT} e^{-hBJ(J+1)/kT}.$$

The line strength becomes

$$S = \frac{8\pi^3\nu^2 hB}{3c(kT)^2}(2J+1)\, e^{-hBJ(J+1)/kT}\left|\mu_{ij}\right|^2 N.$$

The total absorption coefficient at a frequency ν is related to the line strength of a Lorentzian line of width $\Delta\nu_L$ by

$$\gamma_\nu = \frac{S}{\pi}\frac{\Delta\nu_L}{(\nu-\nu_o)^2 + (\Delta\nu_L)^2}.$$

The integrated fractional absorption by the line is given by

$$A = \int_0^\infty (1 - e^{-\gamma_\nu}) d\nu.$$

Ladenberg and Reiche have shown that this integral is

$$A = 2\pi\Delta\nu_L x e^{-x} [J_0(ix) - iJ_1(ix)],$$

where J_0 and J_1 are Bessel functions of the first kind and x is defined by $S/2\pi\Delta\nu_L$.

If $x \ll 1$ the line is unsaturated and $A = S$. If $x \gg 1$ the line is fully saturated and $A = 2(S\Delta\nu_L)^{1/2}$. The line width in most cases is the collision width.

By Kirchhoff's Law, the radiation in a line from a source at temperature T is given by

$$I(\nu) = B_{bb}(\nu,T)A.$$

$I(\nu)$ is the radiation from the line in watts/cm^2 sr. $B_{bb}(\nu,T)$ is the spectral brightness of a black body at temperature T and at frequency ν per unit frequency interval.

REFERENCES

* Work supported by Joint Services Electronics Programs (Contract DAAB07-C-0300), National Science Foundation (Grant GP-24254), and National Aeronautics and Space Administration (Grant NGR 22-009-526).

1. A. A. Penzias and R. W. Wilson, Astrophys. J. 142, 419 (1965).
2. R. H. Dicke, P. J. E. Peebles, P. G. Roll, and D. T. Wilkinson, Astrophys. J. 142, 414 (1965).
3. G. Gamow, in Vistas in Astronomy, ed. by A. Beers (Pergamon Press, New York, 1956), Vol. 2, p. 1726.
4. A. M. Wolfe and G. R. Burbidge, Astrophys. J. 156, 345 (1969).
5. P. E. Boynton, R. A. Stokes, and D. T. Wilkinson, Phys. Rev. Letters 21, 462 (1968).
6. R. B. Partridge and D. T. Wilkinson, Phys. Rev. Letters 18, 557 (1967).
7. E. K. Conklin and R. N. Bracewell, Nature 216, 777 (1967).
8. G. B. Field and J. L. Hitchcock, Phys. Rev. Letters 16, 817 (1966).
9. V. I. Bortolot, Shulman, and P. Thaddeus, to be published.
10. K. Shivanandan, J. R. Houck, and M. O. Harwit, Phys. Rev. Letters 21, 1460 (1968).
11. J. R. Houck and M. Harwit, Astrophys. J. 157, L45 (1969).
12. J. L. Pipher, J. R. Houck, B. W. Jones, and M. Harwit, Nature 231, 375 (1971).
13. A. G. Blair, J. G. Beery, F. Edeskuty, R. D. Hiebert, J. P. Shipley, and K. D. Williamson, Jr., Phys. Rev. Letters 27, 1154 (1971).
14. D. Muehlner and R. Weiss, Phys. Rev. Letters 24, 742 (1970).
15. D. E. Williamson, J. Opt. Soc. Am. 42, 712 (1952).
16. W. Witte, Infrared Phys. 5, 179 (1965).
17. R. Ulrich, Infrared Phys. 7, 65 (1967).
18. D. Muehlner and R. Weiss, in Quarterly Progress Report No. 100, M.I.T. Research Laboratory of Electronics, Jan. 15, 1971 (unpublished), p. 52.

19. B. V. Rollin, Proc. Phys. Soc. (London) 76, 802 (1960).

20. A. Arnaud and G. Quentin, Phys. Letters 32A, 16 (1970).

21. R. W. Keyes, Phys. Rev. 99, 490 (1955).

22. E. K. Gora, J. Mol. Spectroscopy 3, 78 (1959).

23. S. A. Clough, private communication (1970).

24. U. S. Standard Atmosphere Supplements, 1966 (U. S. G. P. O., Washington, D. C., 1967).

25. B. J. Conrath, R. A. Hanel, V. G. Kunde, and C. Prabhakara, J. Geophys. Res. 75, 5831 (1970).

26. W. S. Benedict, private communication (1969).

27. H. J. Mastenbrook, Journal of the Atmospheric Sciences 25, 299 (1968).

28. D. G. Murcray, T. G. Kyle, and W. J. Williams, J. Geophys. Res. 74, 5369 (1969).

29. J. Gay, Astron. and Astrophys. 6, 327 (1970).

30. M. L. Meeks and A. E. Lilley, J. Geophys. Res. 68, 1683 (1963).

31. H. A. Gebbie, W. J. Burroughs, and G. R. Bird, Proc. Roy. Soc. A. 310, 579 (1969).

32. E.g., see C. H. Townes and A. L. Schawlow, Microwave Spectroscopy (McGraw-Hill Book Co., Inc., New York, 1955).

33. J. S. Seeley and J. T. Houghton, Infrared Phys. 1, 116 (1961).

34. A. H. Barrett, private communication (1971).

35. C. B. Leovy, J. Geophys. Res. 74, 417 (1969).

36. D. J. Hegyi, W. A. Traub, and N. P. Carleton, to be published.

37. M. Harwit, private communication (1972)

FIGURE CAPTIONS

1. Schematic diagram of the apparatus.
2. The radiometer.
3. Transmission spectra at 4.2° of some optical components of the radiometer. The relative detector responsivity vs. frequency is also shown, as well as the transmission spectrum of a sample of the InSb detector material.
4. The five spectral responses of the instrument.
5. The spectral responses multiplied by the frequency squared.
6. The radiometer beam profile in each of the spectral responses.
7. Annular response and the effective solid angle within θ vs. θ.
8. Detector bias voltage and responsivity vs. bias current. The curves labeled "coil in" include the voltage step-up due to the RLC circuit at a chopping frequency of 2.1 kHz; those designated by "no coil" show the response of the detector without the RLC circuit.
9. The black body used for laboratory calibration of the radiometer.
10. Radiometer calibration curves.
11. The balloon package ready for launching (June).
12. Inflight photographs of the apparatus (September).
13. Inflight calibration signals vs. time (September).
14. Radiometer signal vs. zenith angle (September).
15. Calculated radiation from atmospheric constituents at 39 km.
16. Atmospheric pressure at the radiometer during ascent (September).
17. Radiometer signal in SR1 vs. pressure during ascent (September).
18. Summary of far infrared background measurements.
19. Region of sky observed (September).

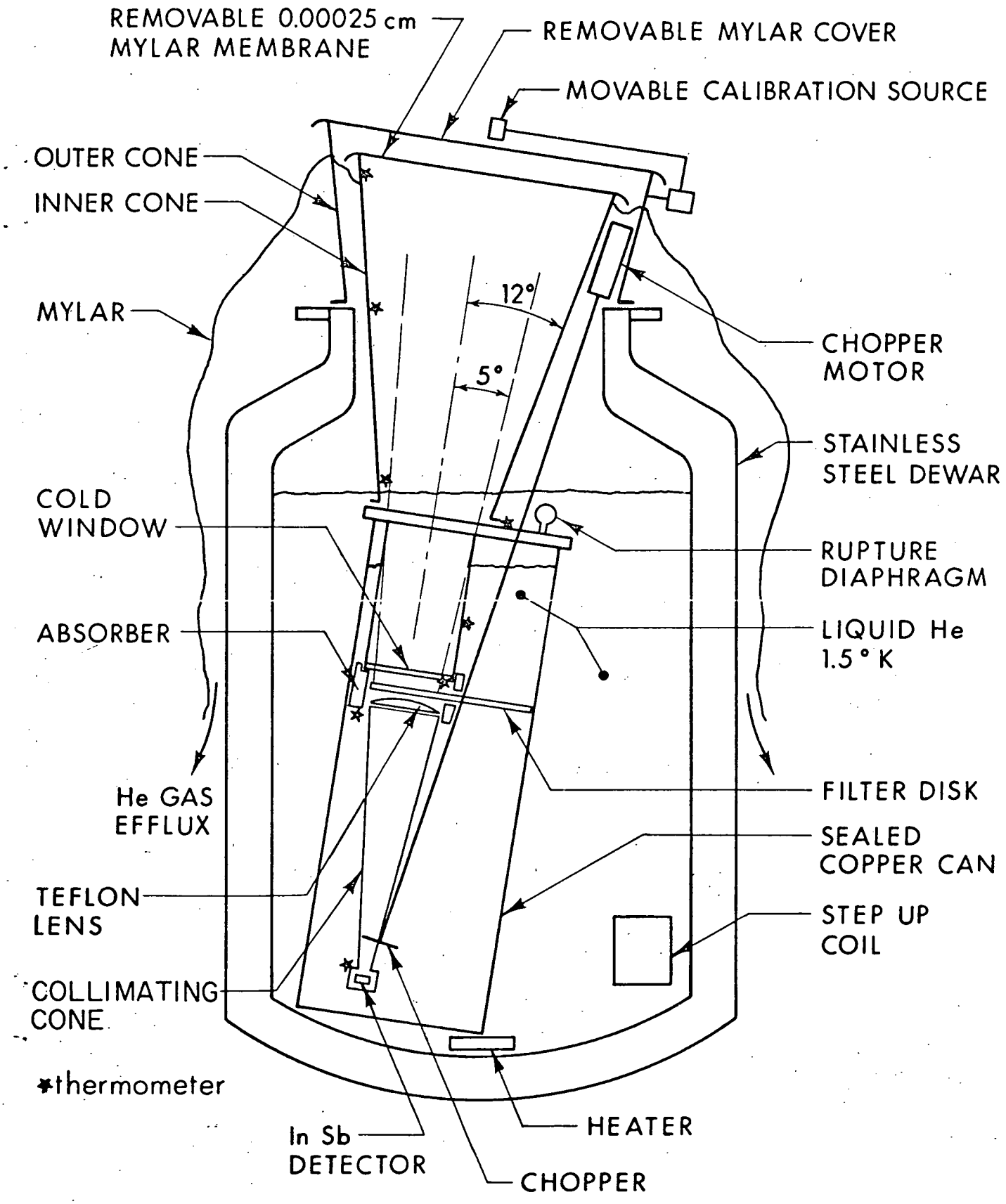

1. Schematic diagram of the apparatus.

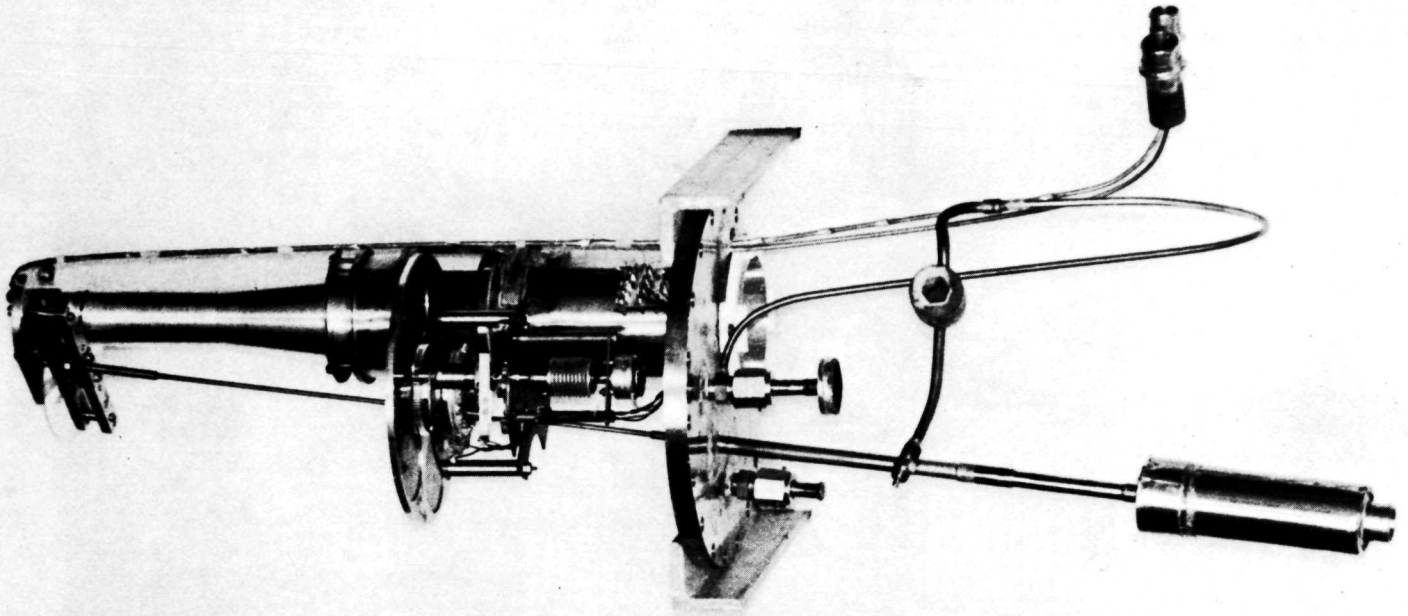

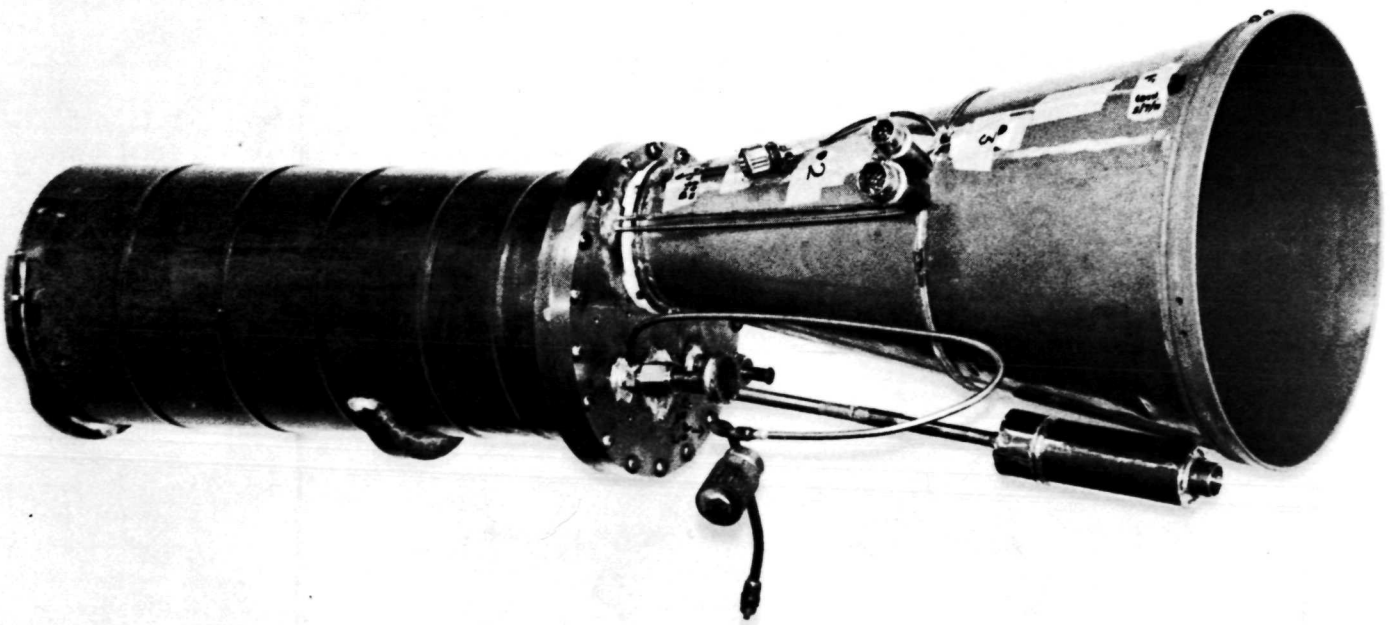

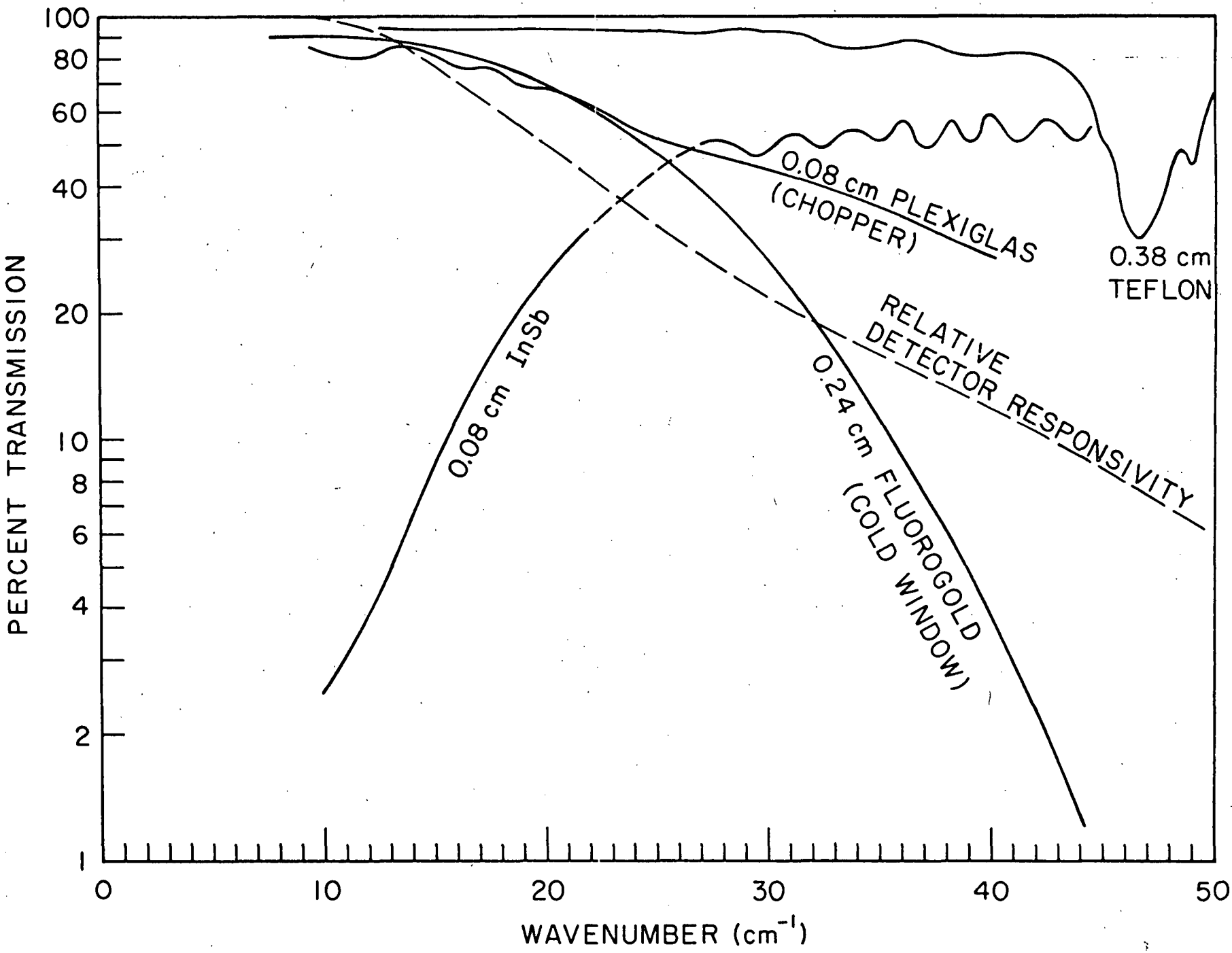

3. Transmission spectra at 4.2° of some optical components of the radiometer. The relative detector responsivity vs. frequency is also shown, as well as the transmission spectrum of a sample of the InSb detector material.

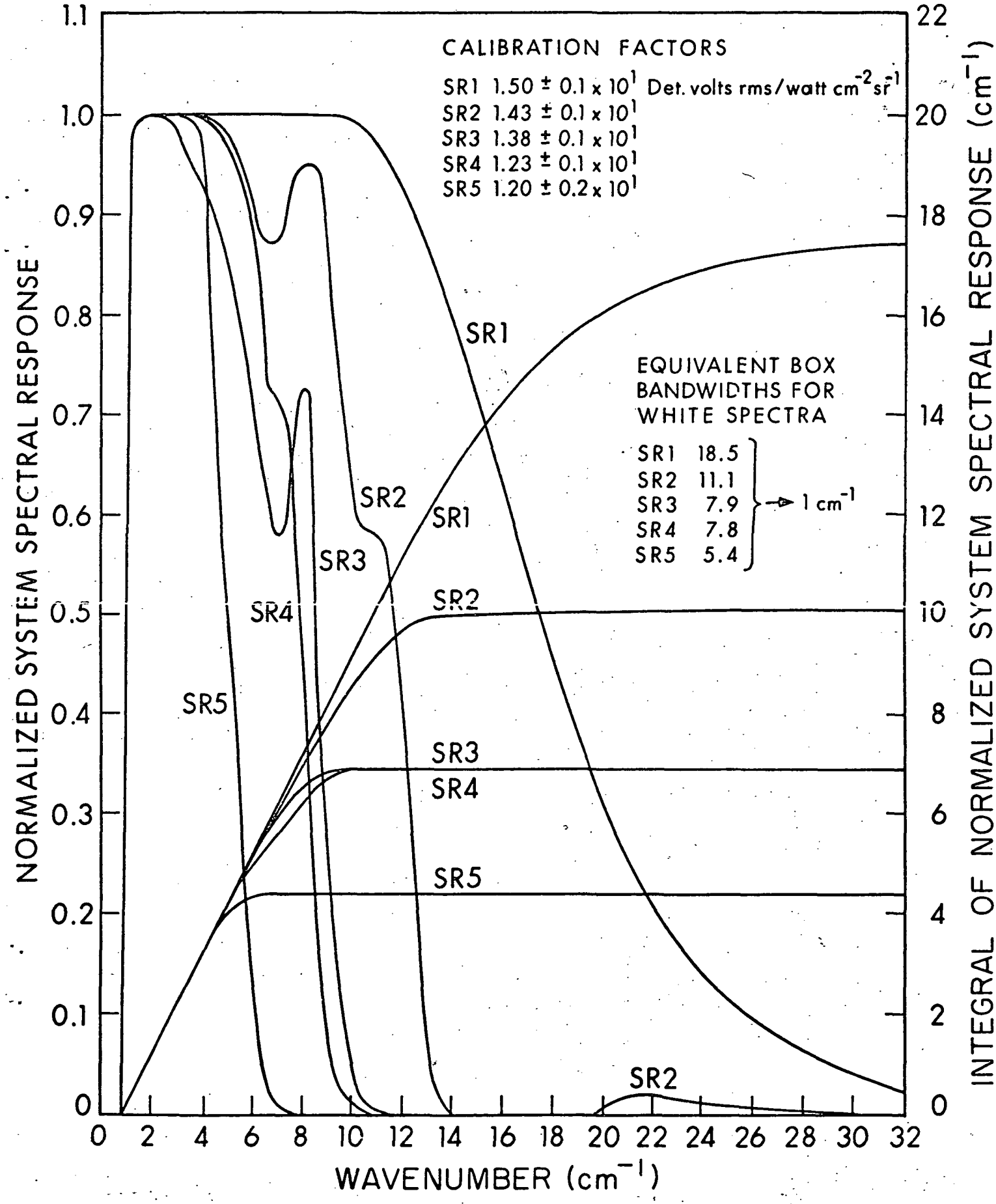

4. The five spectral responses of the instrument.

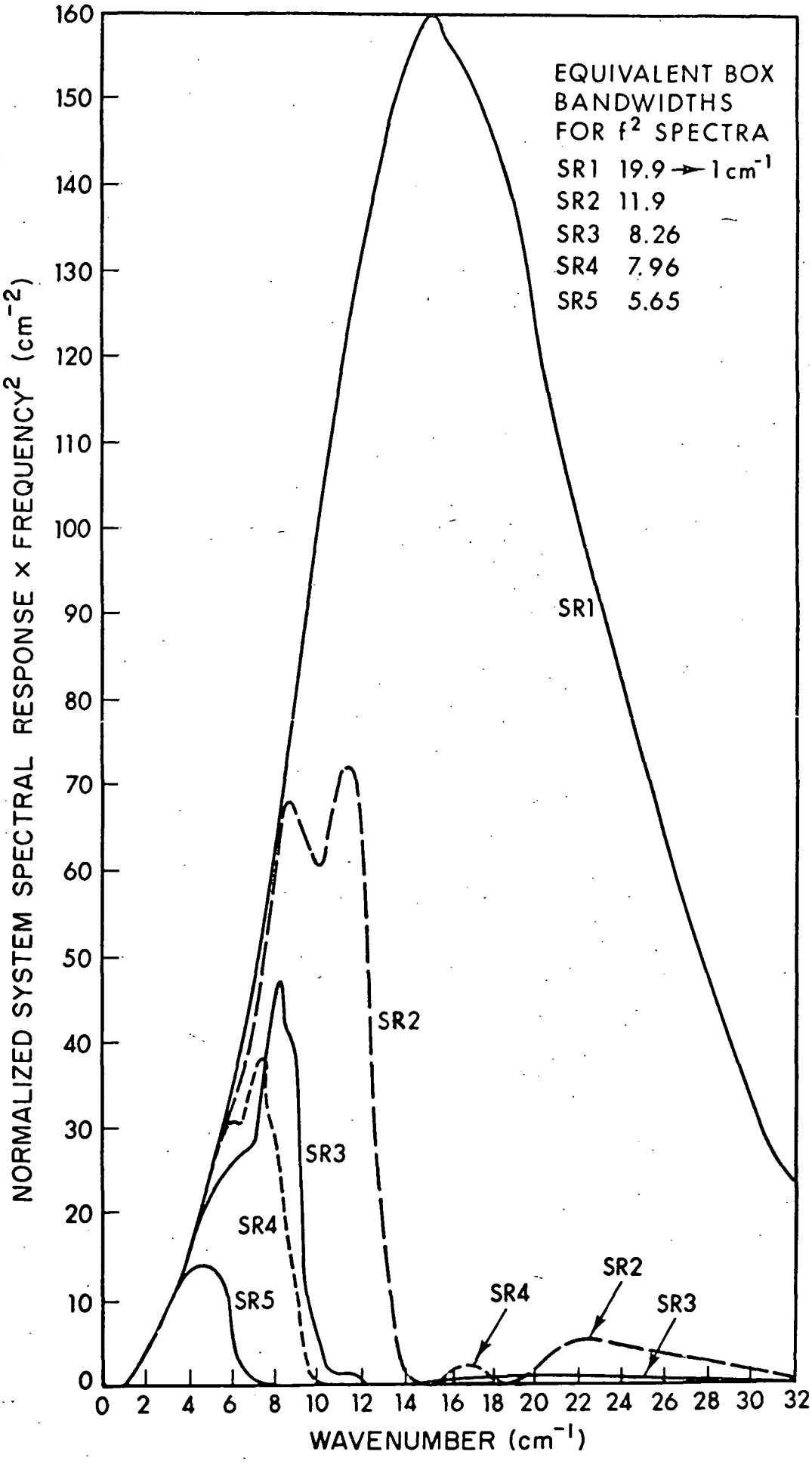

5. The spectral responses multiplied by the frequency squared.

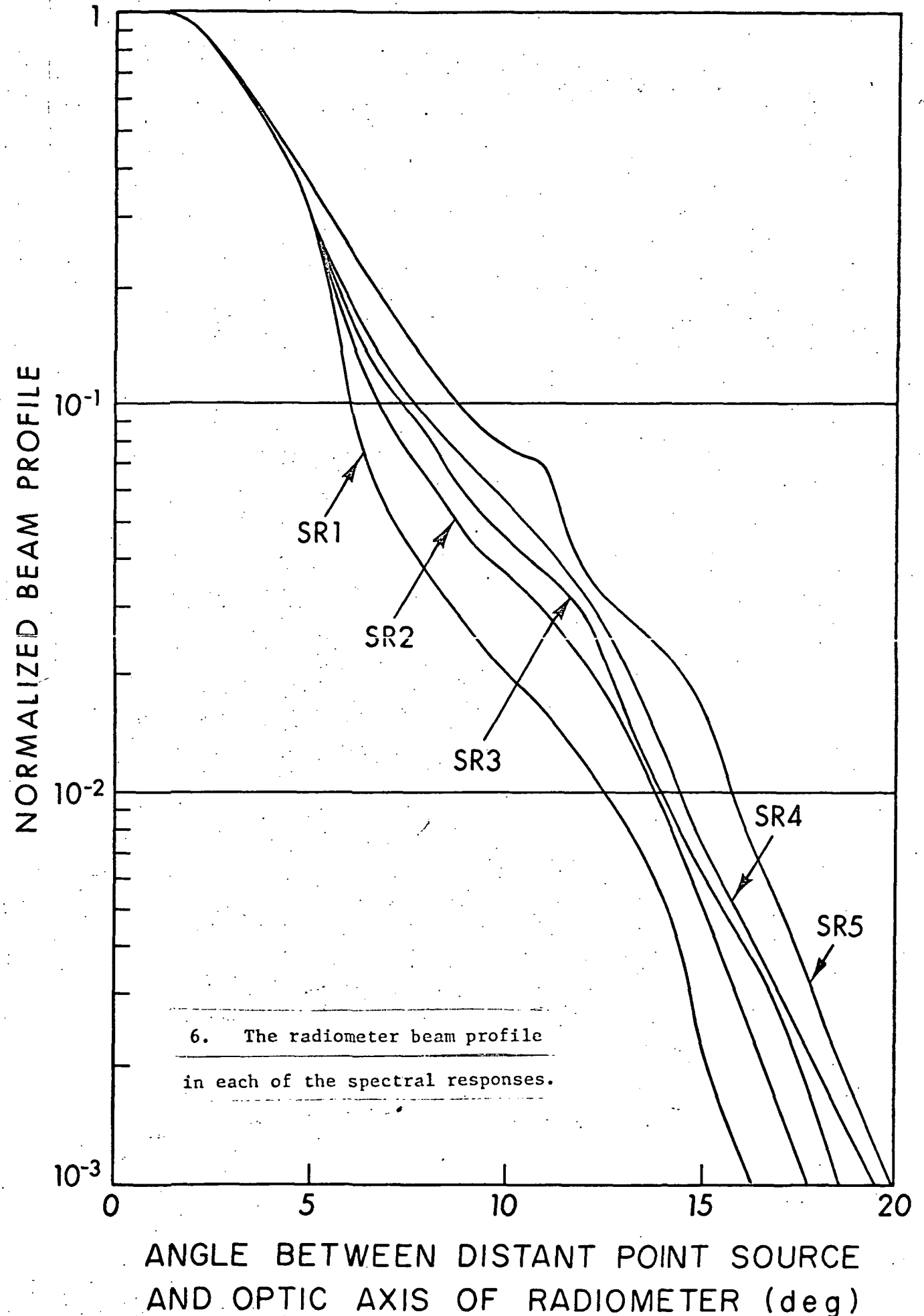

6. The radiometer beam profile in each of the spectral responses.

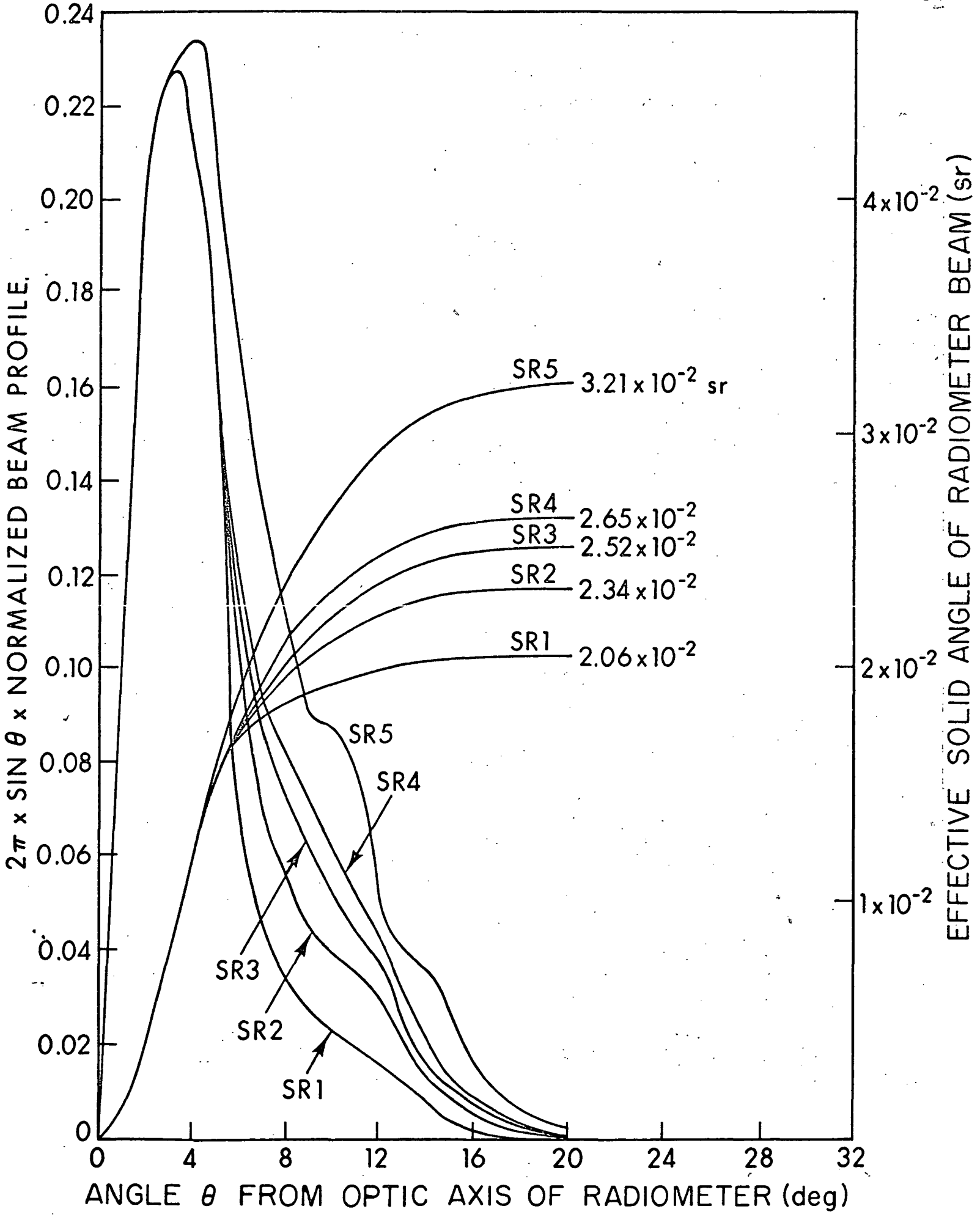
0.24
0.22
0.20
0.18
0.16
0.14
0.12
0.10
0.08
0.06
0.04
0.02
0
2π x SIN θ x NORMALIZED BEAM PROFILE
4x10-2
3x10-2
2x10-2
1x10-2
EFFECTIVE SOLID ANGLE OF RADIOMETER BEAM (sr)
SR5 3.21x10-2 sr
SR4 2.65x10-2
SR3 2.52x10-2
SR2 2.34x10-2
SR1 2.06x10-2
SR5
SR4
SR3
SR2
SR1
0
4
8
12
16
20
24
28
32
ANGLE θ FROM OPTIC AXIS OF RADIOMETER (deg)

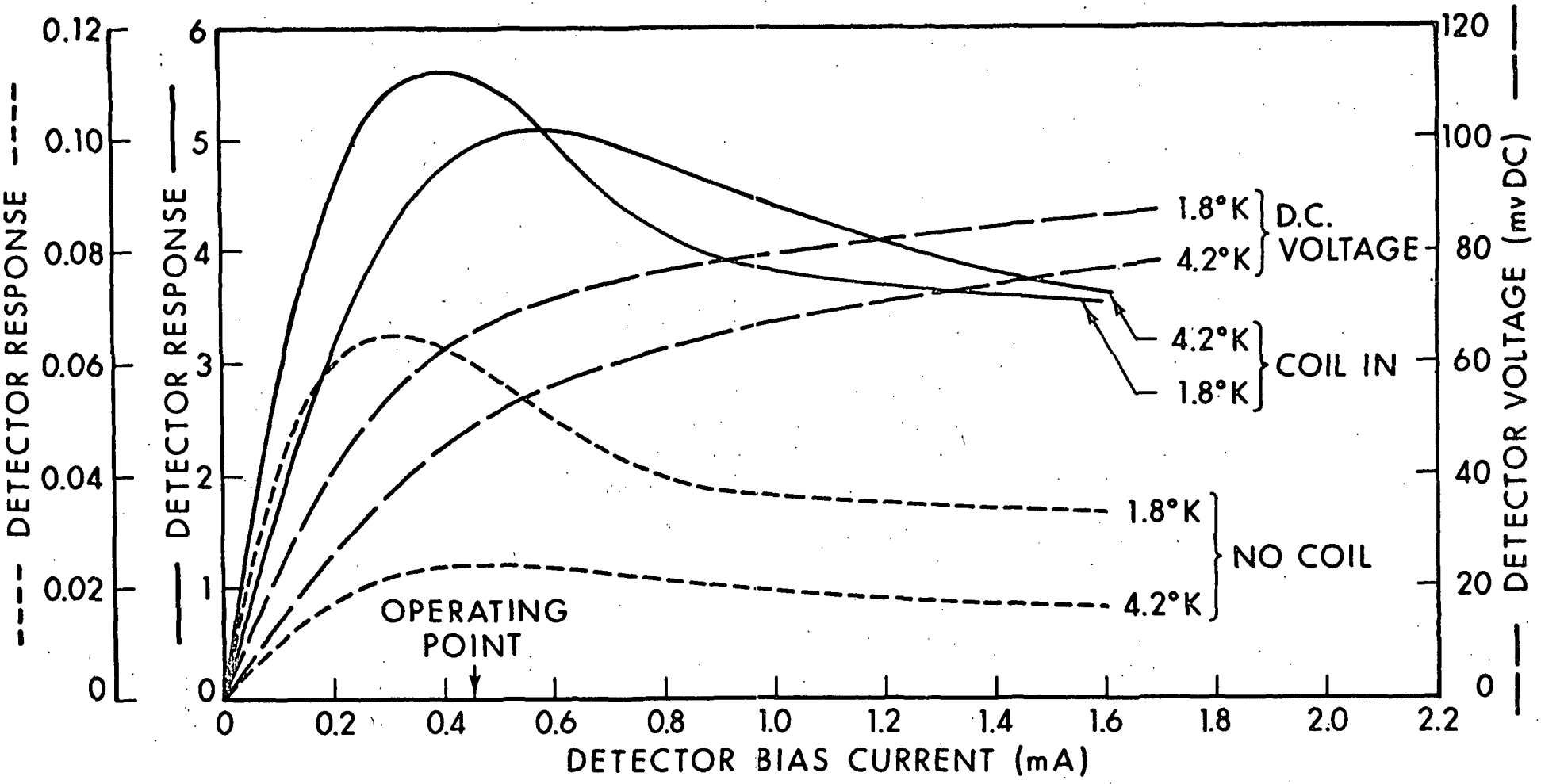

8. Detector bias voltage and responsivity vs. bias current. The curves labeled "coil in" include the voltage step-up due to the RLC circuit at a chopping frequency of 2.1 kHz; those designated by "no coil" show the response of the detector without the RLC circuit.

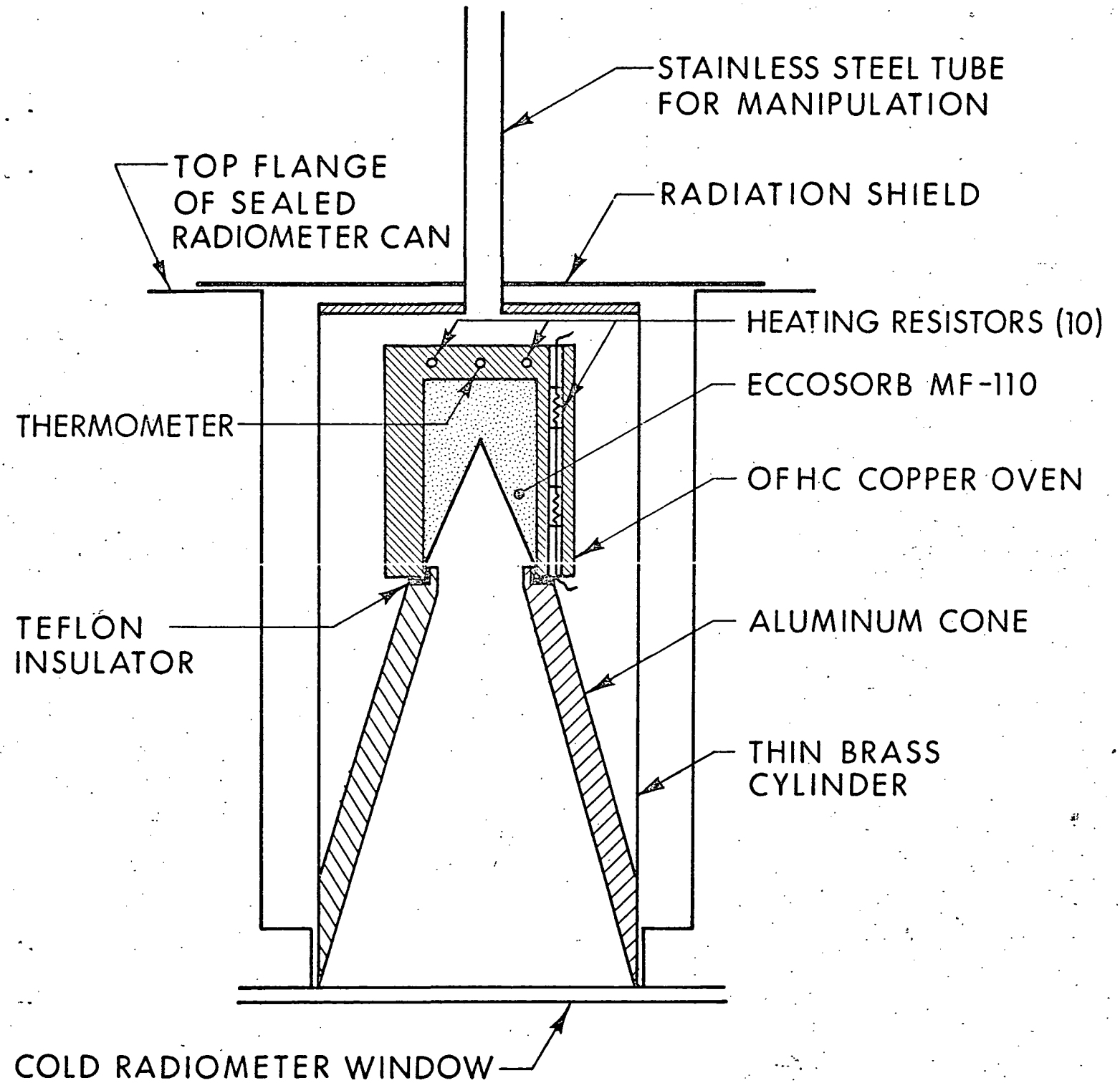

9. The black body used for laboratory calibration of the radiometer.

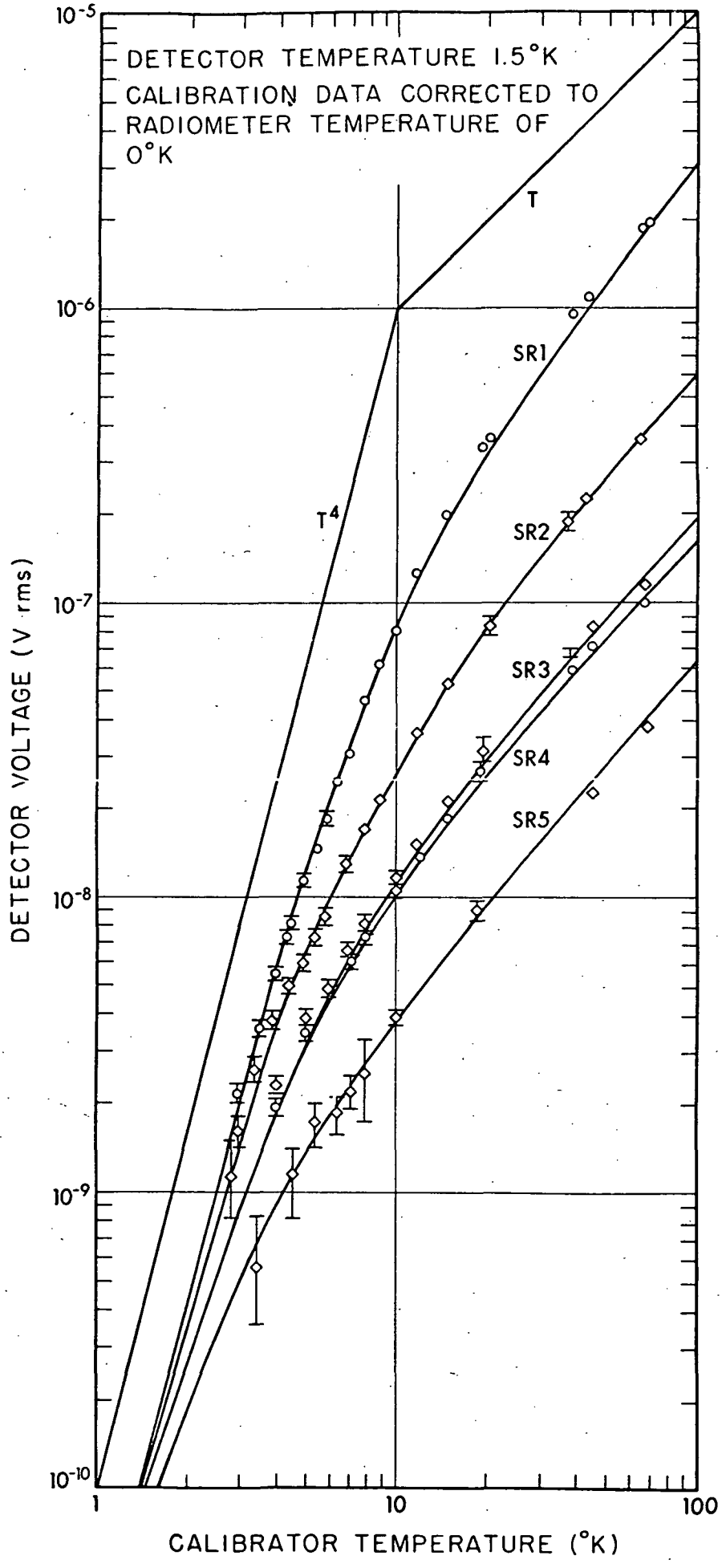

10. Radiometer calibration curves.

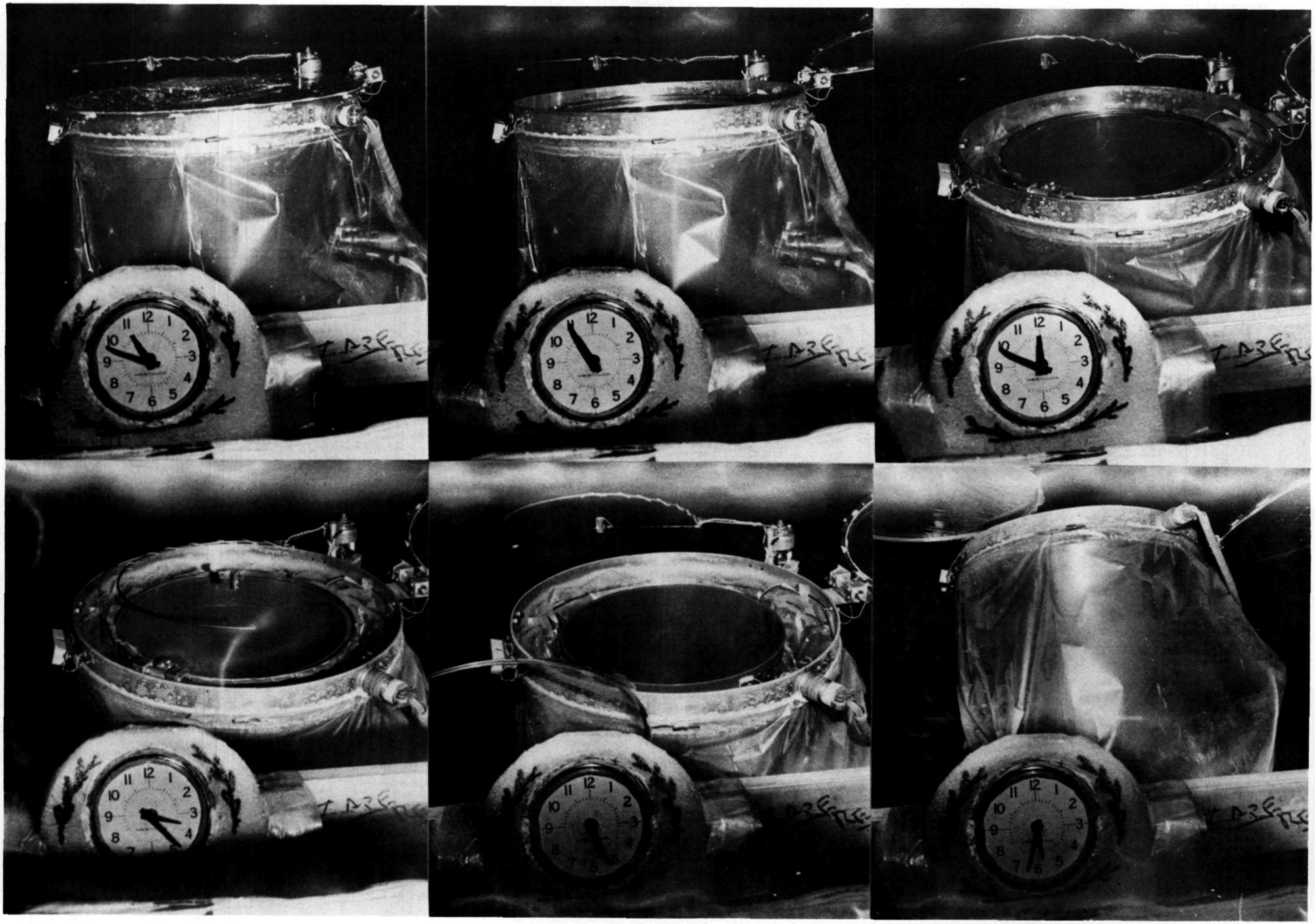

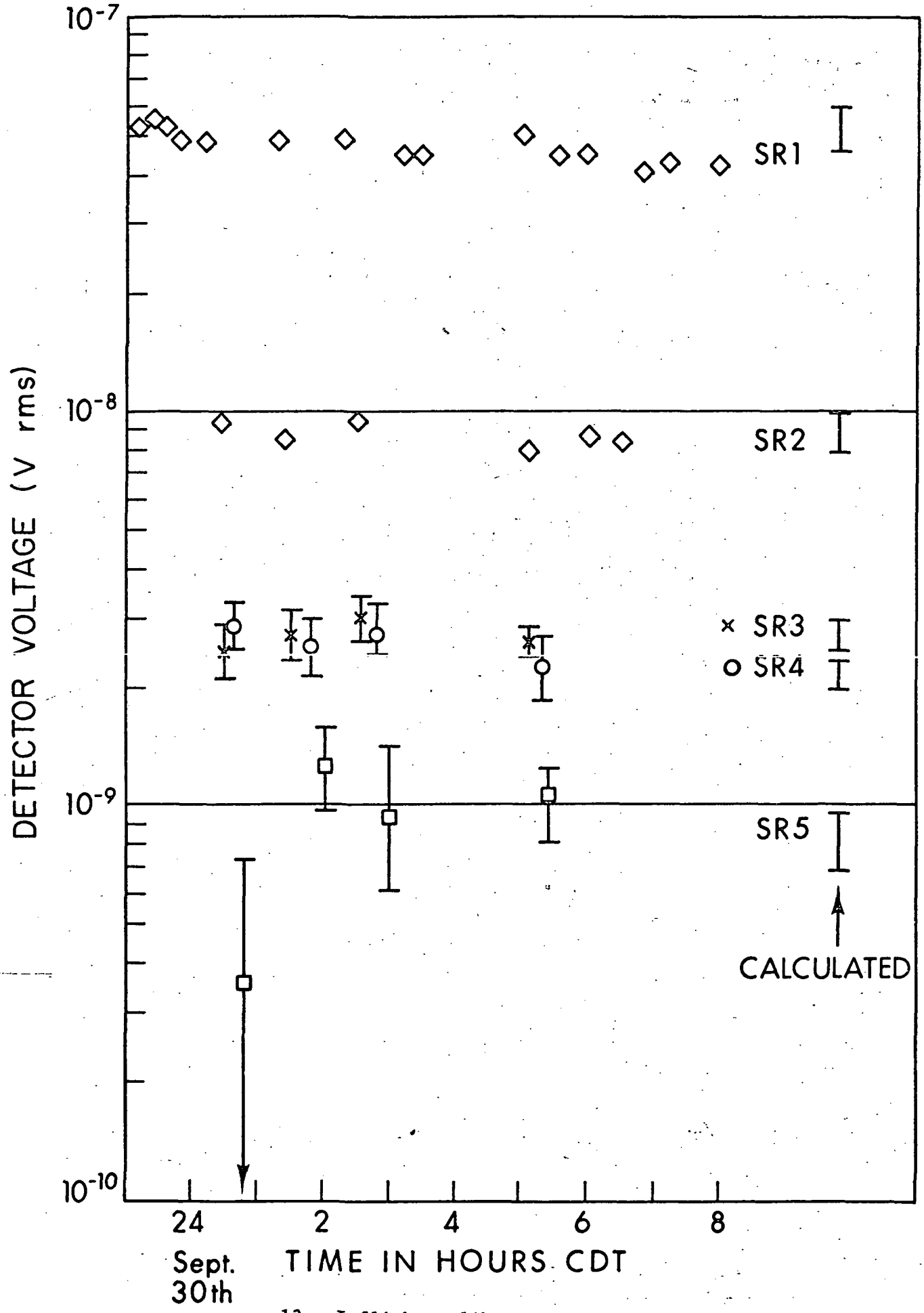

13. Inflight calibration signals vs. time (September).

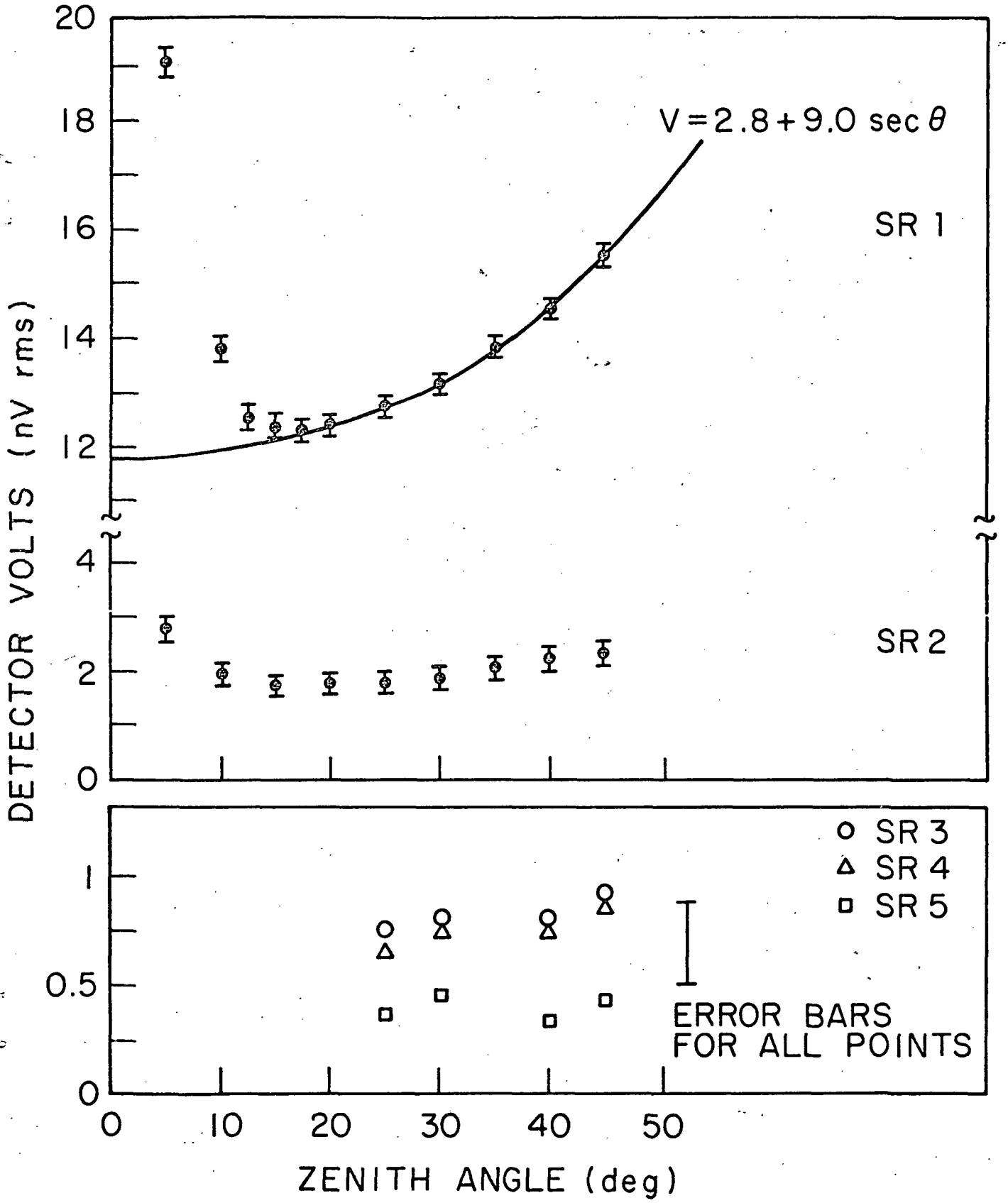

14. Radiometer signal vs. zenith angle (September).

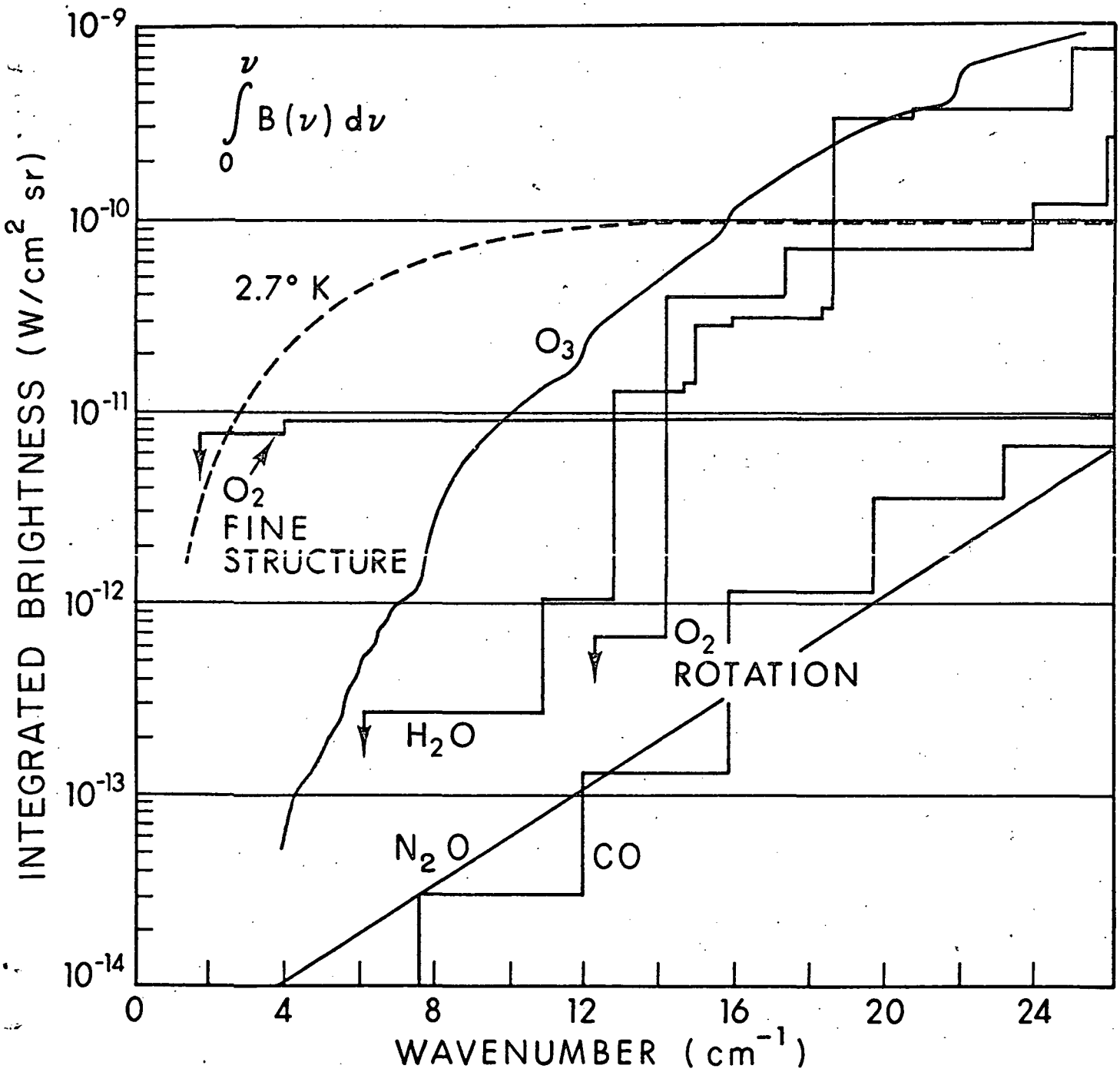

15. Calculated radiation from atmospheric constituents at 39 km.

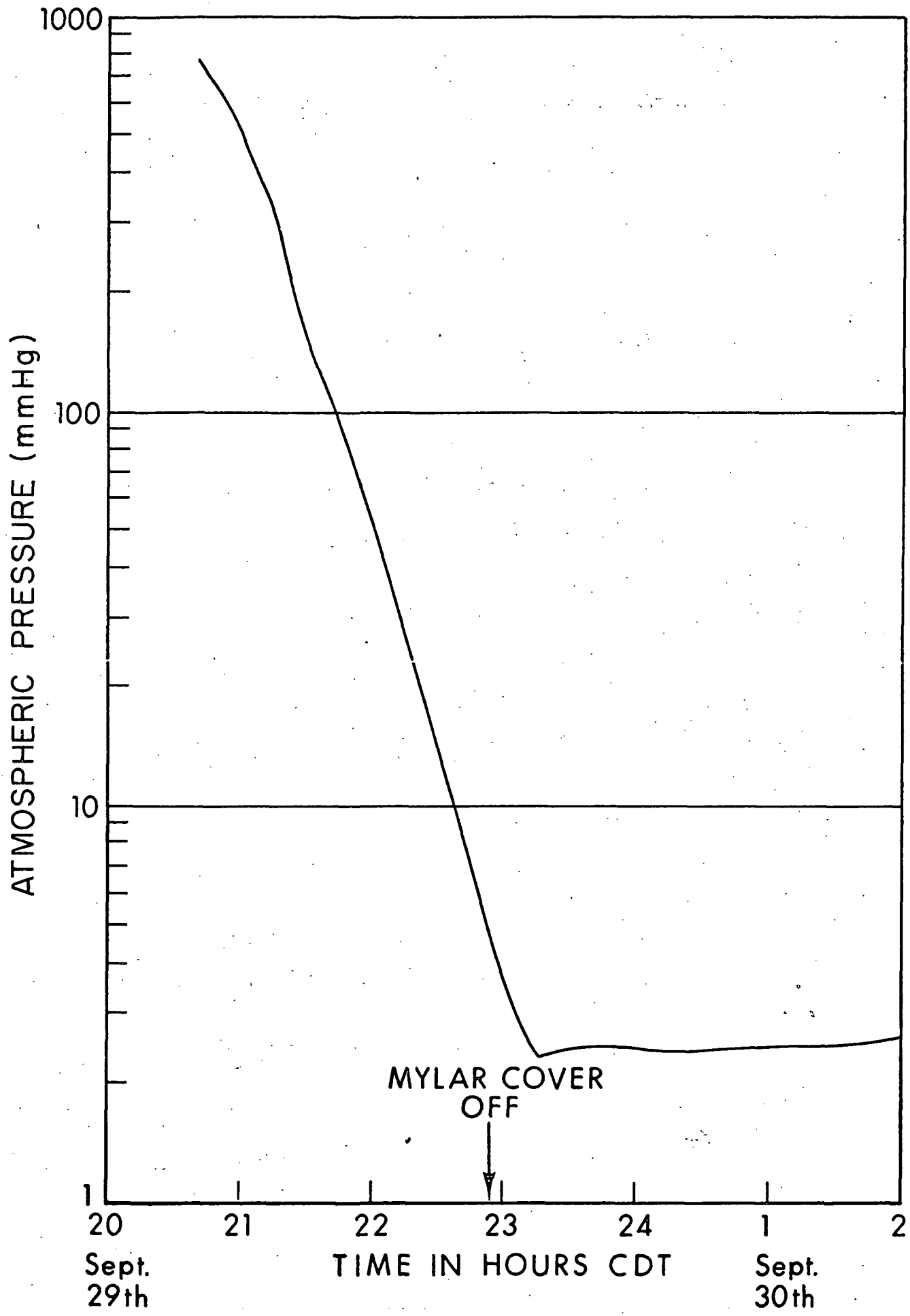

16. Atmospheric pressure at the radiometer during ascent

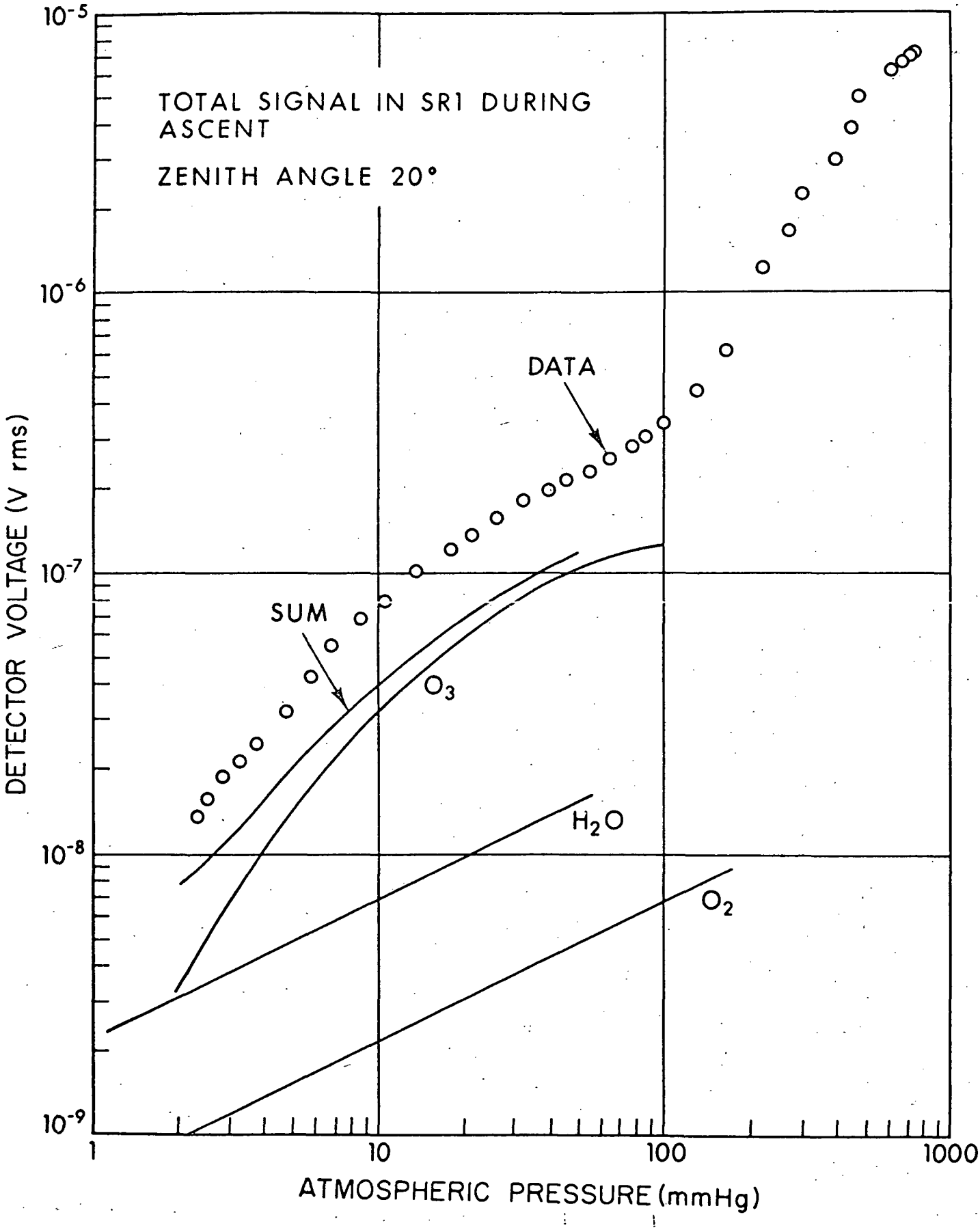

17. Radiometer signal in SR1 vs. pressure during ascent (September).

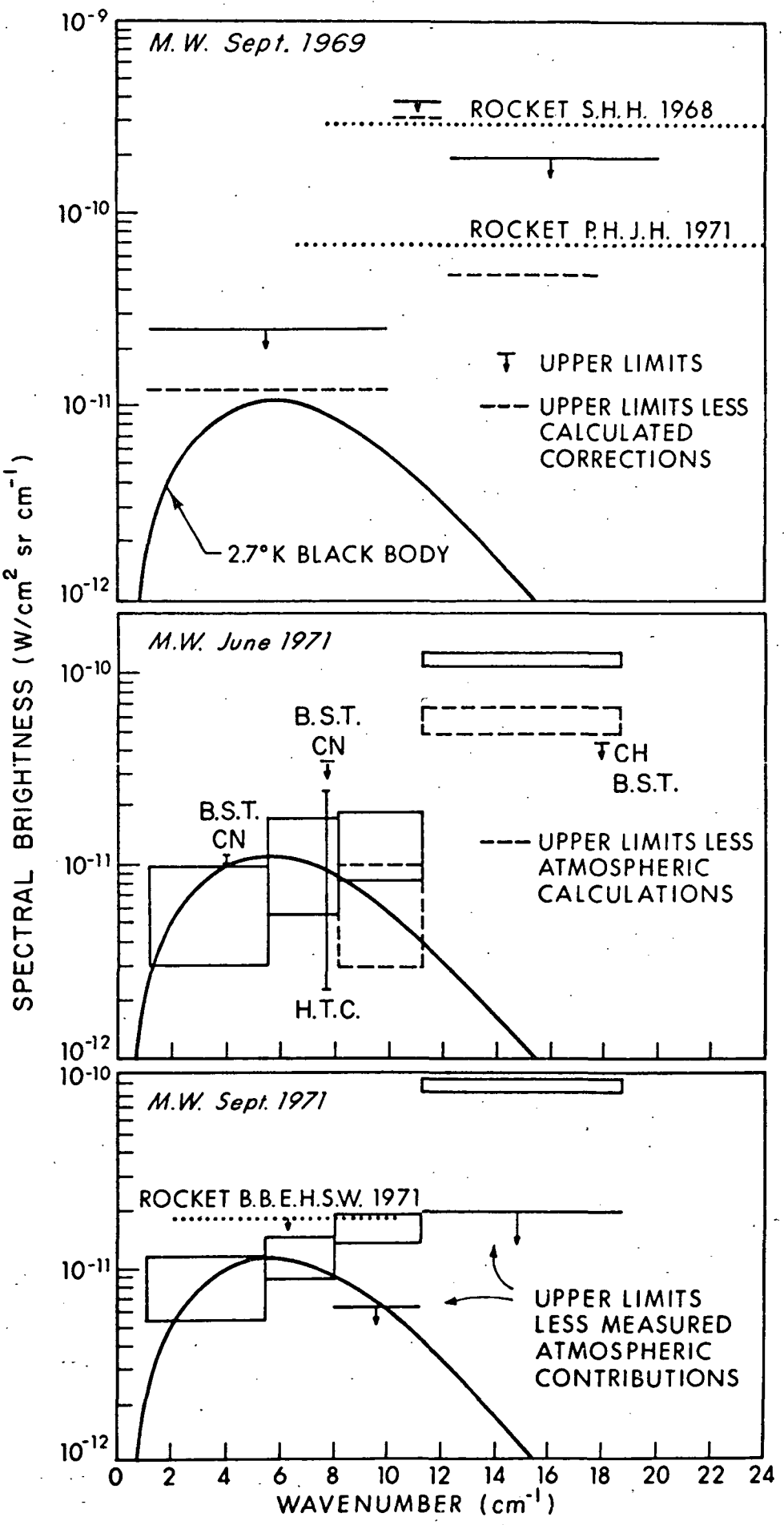

18. Summary of far infrared background measurements.

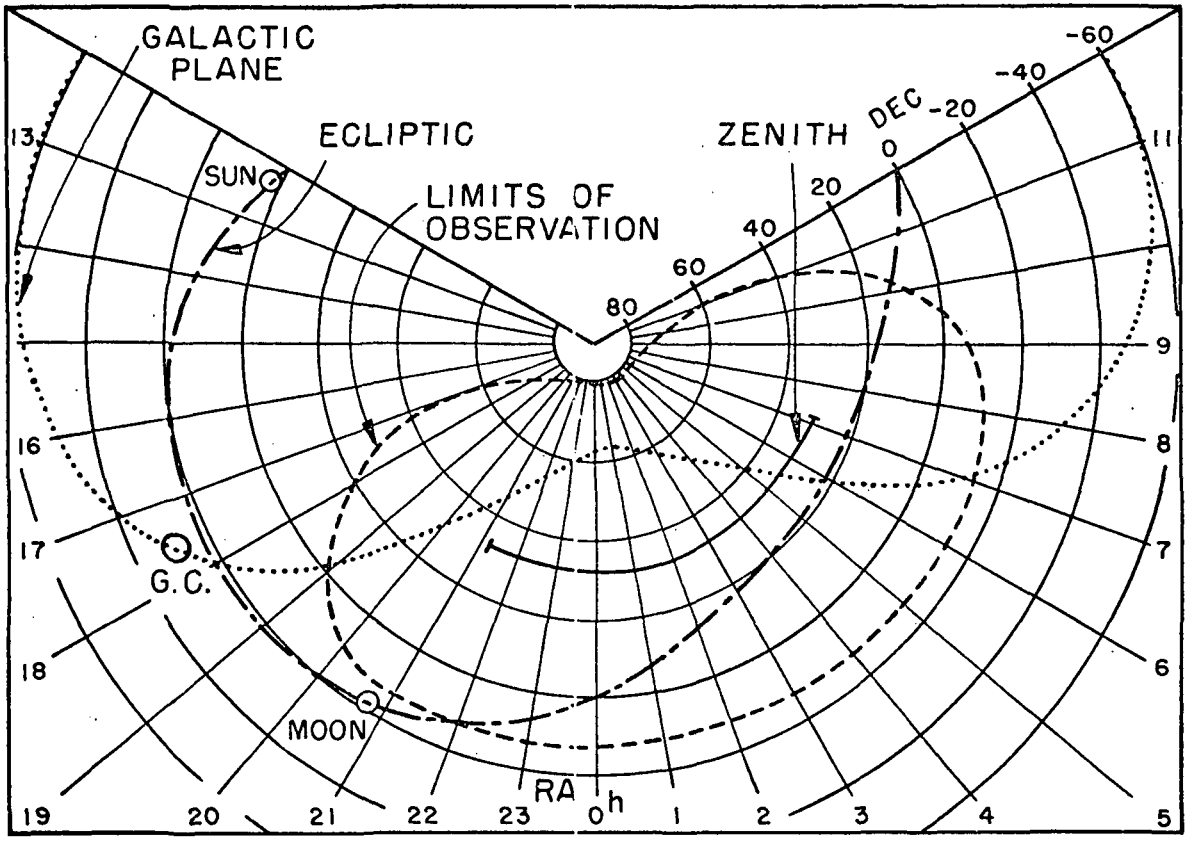

19. Region of sky observed (September).